**Universität Stuttgart**

**Geodätisches Institut**

# Surface Deformation Analysis of GPS Dense Networks based on Intrinsic Approach

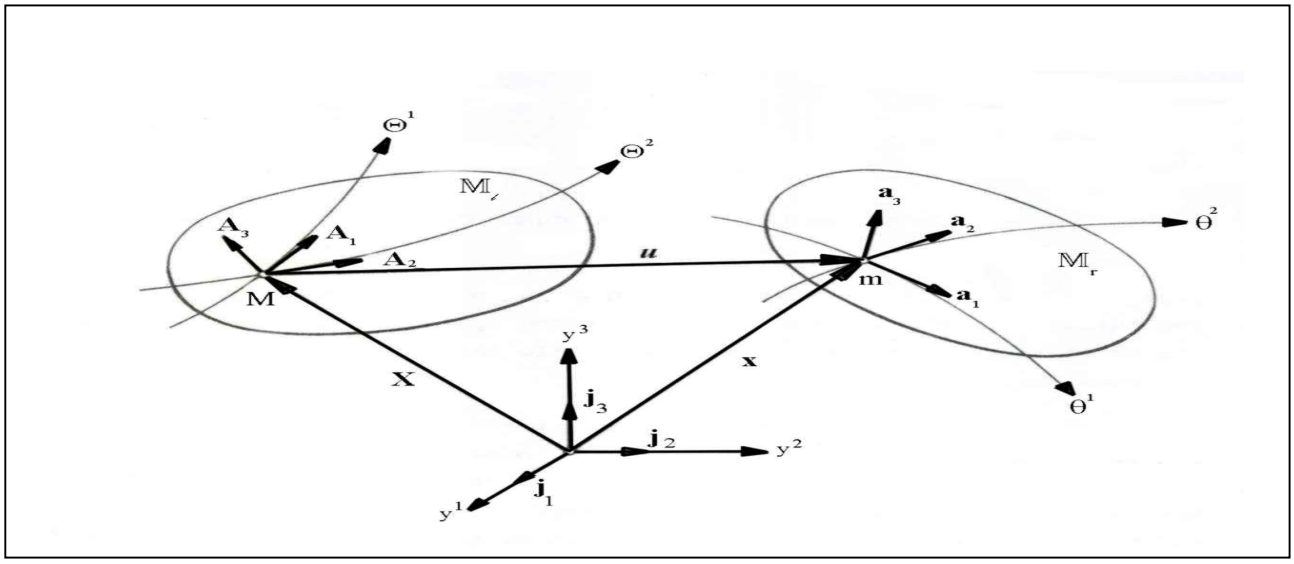


Diplomarbeit im Studiengang

**Geodäsie und Geoinformatik**

an der Universität Stuttgart

Khosro Moghtasad-Azar

Stuttgart, Januar 2007

**Betreuer:**

Prof. Dr.-Ing.habil. Dr.techn.h.c. mult. Erik W. Grafarend
Universität Stuttgart

Dr.-Ing. Jianqing Cai
Universität Stuttgart

## Abstract

Here we present a method of differential geometry, an intrinsic approach that allows deformation analysis of the real surface of the Earth on its own rights for a more reliable and suitable estimate of the surface deformation measures. The method takes advantage of the simplicity of the *two-dimensional Riemannian manifold spaces* $\mathbb{M}^2$ versus the *three dimensional Euclidean* spaces $\mathbb{E}^3$ without losing or neglecting information and effect of the third dimension in the results.

Here we describe the regularized Earth's surface as a graded *two-dimensional Riemann manifold* $\mathbb{M}^2$, namely a curved surface, embedded in a *three dimensional Euclidean space* $\mathbb{E}^3$. Thus, deformation of the surface can be completely specified by the *change of the first and second fundamental tensors*, namely *changing of metric tensor and changing of curvature tensor*, of the surface, which *changing of curvature tensor* is responsible for detection of vertical displacements on the surface.

This study describes analytical modelling, derivation, and implementation of the surface deformation measures based on the proposed method, particular attention to the formulation and implementation of the *tensors of rotation* and *tensor of change of curvature* in Earth deformation studies. The method is applied to a real data set of dense space geodetic positions and displacement vectors across the *Southern California*. A comparison of the patterns with the geological and geophysical evidences of the area indicated how well the patterns were able to reveal different geodynamical features of the region.

## Zusammenfassung

In dieser Arbeit stellen wir eine Methode der Differentialgeometrie basierend auf einem spezifischen Ansatz intrinsischen Flächenmethode vor, die es erlaubt, eine Deformationsanalyse der wahren Erdoberfläche mit zuverlässigeren und passenden Schätzungen der Deformationsmaße durchzuführen. Das Verfahren nutzt die Einfachheit der zweidimensionalen Riemann'schen Mannigfaltigkeit $\mathbb{M}^2$ gegenüber den dreidimensionalen Euklidischen Räumen $\mathbb{E}^3$ aus, ohne Information und den Effekt der dritten Dimensionen in den Ergebnissen zu verlieren oder zu vernachlässigen.

Wir beschreiben die regularisierte Erdoberfläche als eine abgestufte zweidimensionale Riemann'sche Mannigfaltigkeit $\mathbb{M}^2$, speziell eine gekrümmte Oberfläche, die in den dreidimensionalen Euklidischen Raum eingebettet ist. Aus diesem Grunde kann die Deformation einer Oberfläche vollständig durch die Veränderung der ersten und zweiten Fundamentalformen der Fläche, also der Veränderung des Metriktensors und des Krümmungstensors, erfasst werden, wobei die Veränderung des Krümmungstensors verantwortlich für die Ermittlung vertikaler Deformationen der Oberfläche ist.

Diese Studie beschreibt die analytische Modellierung, Herleitung und Umsetzung der Deformationsmaße basierend auf der vorgeschlagenen Methode, wobei der Formulierung und Umsetzung der Rotationstensoren und des Tensors der Krümmungsänderung für Deformationsanalysen besondere Aufmerksamkeit geschenkt wird. Die Methode wurde auf einen Realdatensatz, der aus mit geodätischen Raumverfahren bestimmten, dichten Positionen und Verschiebungsvektoren in der Region von Südkalifornien besteht, angewendet. Ein Vergleich der bestimmten Muster mit den geologischen und geophysikalischen Gegebenheiten des Gebietes zeigt, wie gut die Muster die verschiedenen geodynamischen Eigenschaften dieser Region offen legen können.

## Acknowledgments

I would like to express my sincere gratitude to my supervisor, *Prof. Dr.-Ing. habil. Erik W. Grafarend,* for introducing this fascinating topic to me and whose tireless efforts and patience as my supervisor greatly contributed towards the completion and success of this study at the Institute of Geodesy - Faculty of Aerospace Engineering and Geodesy, University of Stuttgart.

My hearty thanks also go to *Dr.Cai* for reviewing the work with great care and providing many helpful comments and suggestions that further improved this dissertation.

I am grateful of the members of the Department of Geodesy- Faculty of Aerospace Engineering and Geodesy, University of Stuttgart, for each of them contributed in one way or another towards the success of my research work.

I wish to acknowledge gratefully the financial support from the Ministry of Culture and Higher Education of Iran for sponsoring this study.

Last, but not least, I wish to acknowledge the patience of my wife *Zhaleh Safarpour* and my son *Ataeollah Moghtased Azar* for all their unsparing support and understanding.

## Contents

## List of Figures

## List of Boxes

# Chapter 1

# Introduction

Following the classical separation of established geodetic techniques, namely triangulation and trilateration versus levelling, deformation of the Earth's surface has been separated into horizontal and vertical components and has been treated individually. The main reason for this conventional separate procedure is due to the horizontal and vertical networks in classical geodesy. Later space geodesy, such as *GPS*, *VLBI*, *SLR*, and *DORIS* has changed the rules of the game of positioning essentially. Positions of network points, containing both horizontal and vertical components, could be determined with high precision, enough to be used as an accurate and reliable source of information in Earth deformation studies. The great number of studies of this type using displacement fields derived from repeated observations of space geodetic networks indicates how valuable and important role the space geodetic techniques play in present and future states of geodynamics. A sample reference of surface deformation studying let us take notice of: *Ahjos et al.*,(1992), *Argus et al.*, (1989), *Bada et al.*, (1999), *Bianco et al.*, (1998), *Bock* et al., (1989), *Boucher et al.*, (1999), *Caporali et al.*, (2000) , *Castellarin et al.*, (1992), *Chen* (1991),*Chan et al.*,(2006) , *Clarke et al.*, (1998), *Cross et al.*,(1987), *DeMets et al.*, (1999), *Dewey* (1988), *Gasparini et al.*, (1985), *Goelke et al.*,(1996), *Harada et al.*,(1978), *Horner et al.*, (1983), *James et al.*, (1993), *Kahle et al.*, (1998), *Kakkuri et al.*, (1992), *Kakkuri* (1997), *Kakkuri et al.*, (1998), *Lesne et al.*, (1998), *Livieratos* (1978), *Lundgren et al.*, (1995),*MacMillan et al.*, (1999), *McCarthy* (1996), *McKenzie* (1970), *Miyazaki et al.*, (1997), *Mueller et al.*, (1994), *Pagarete et al.*, (1998), *Plag et al.*, (1998), *Reilinger et al.*, (1997a, 1997b), *Renner* et *al.*, (1994), *Sagiya et al.*, (1999), *Scherneck et al.*, (1998), *Smith et al.*,(1990), *Soudarin et al.*,(2006) ,*Terada et al.*, (1929), *Tregoning et al*. (1998), *Tsuboi* (1930), *Vanbrabant et al.*, (1999), *Vanıcek et al.*, (1981), *Ward* (1998a,b), *Wessel et al.*, (1998) ,*Wu* (1998).

Despite the ability of space geodesy to provide 3-dimensional displacement fields, the crustal deformation studies are still carried out separately in horizontal and vertical components. The main reason of the separation is claimed to be the non-sufficient accuracy of height component of point position. However some people use also the third components of *GPS* measurements in order to

detection of vertical deformations of the crust when they have continuous recording of *GPS* measurements for several years, namely not campaign measurements. For instance, *J.M. Johansson et al*., (2002), *G.A Milne et al.,* (2001) used of vertical component of *GPS* for detection of vertical deformation in the *BIFORST* (*Baseline Inferences for Fennoscandian Rebound Observations Sea Level and Tectonic)* project, *Mazzotti et al*., (2003) on vertical deformation over the north of *Cascadia*, *Aoki* et al., (2003) on vertical deformation over *Japan*, *Beavan* et al., (2004) on vertical deformation over the Southern *Alps*, and so on.

Traditional crustal motions and deformations are described as elements of 3-*dimensional Euclidean space* $\mathbb{E}^3$. Regarding the fact that in reality, crustal motions and deformations are embedded in a *3-dimensional Euclidean space* and do not exist purely horizontal or purely vertical in terms of deformations.

In the last two decades, some efforts have been made to formulate the problem in *3-dimensional embedding Euclidean space*. *J. Zaiser* (1984) computes the displacement field, the strain field and the rotation field in the context of arbitrary shaped geodetic networks and *three-dimensional finite elements*. A curvilinear *three-dimensional finite element method* is introduced by *E. W. Grafarend* (1986) for representation of local strain and local rotation tensors in terms of ellipsoidal, *Gauss-Krüger* or *UTM* coordinates. A study of the estimability-invariance characteristics of deformation parameters obtained through the *finite element method* by using a dimension free approach with results that can be immediately specialized to three or two dimensions, has been carried out by *A. Dermanis and E. W. Grafarend* (1993).

Thus, the modelling of the problems connected with deformations in 3-dimensions *Euclidean* space by computing separately the 2- dimensional planar deformations and vertical motions cannot portray the real state of crustal deformations. On the other hand, the *3-dimensional Euclidean space* methods of Earth deformation analysis lose the simplicity of computations in *2-dimensional manifold spaces*.

Moreover, interpretation of the result of the analysis, namely 3-dimensional deformation tensors and particularly invariants associated with them, *is not an easy task*.

The two-dimensional plane deformation analysis of the crust is limited to investigation of the alteration of the metric characteristics of the crust. In other words, the analysis allows us to bring the *metric tensors* of the two states of the body into a *one-to-one* correspondence. The Earth surface deformations can't be completely specified by the change of the *metric tensor*, as a *two dimensional Riemannian manifold* which is embedded in *three dimensional Euclidean space*.

These facts indicate the need for reevaluation of the theoretical foundations of the Earth deformation analysis methods. Regarding these disadvantages and difficulties as well as the fact that we have only *surface geodetic measurements* in our hands, it seems that a surface approach in the Earth's surface deformation analysis based on *3-dimensional Euclidean* displacement fields is an appropriate solution. In other words, an approach that keeps the simplicity of computations in *2-dimensional curvilinear spaces* includes both vertical and horizontal components of the Earth deformations, and refers to the real surface of the Earth will be able to resolve the problems of the existing methods [*Grafarend et al*., 2003].

This study presents an analytical formulation and implementation of a method of Earth's surface deformation analysis referring to the real surface of the Earth. We benefit from the mathematical models and tools of *surface deformation analysis* in shell theory [*Mushtari et al*., 1961, *Naghdi* 1972, *Reissner* 1974, *Pietraszkiewicz* 1977, *Olszak* 1980, *and Libai* 1998], differential geometry of surfaces, in order to develop appropriate modelling of deformations on the Earth's surface. Here we describe the Earth's surface as a 2-*dimensional Riemann manifold* $\mathbb{M}^2$, namely a curved surface, embedded in a *3-dimensional Euclidean space* $\mathbb{E}^3$. Thus, deformation of the surface can be completely specified by the *change of the first and second fundamental tensors*, namely *changing of metric tensor and changing of curvature tensor*, of the surface, which *changing of curvature tensor* is responsible for detection of vertical displacements on the surface. Special emphasis is given to definition of proper invariants of the introduced surface deformation tensors with meaningful physical interpretations.

Following the conventions of continuum mechanics, all the coordinates related to *reference* state are printed in *capital letters* and coordinates related to *current* state are printed in the *small letters*. Hence, we apply the *summation convention* over the repeated indices and an index printed in *Greek letter* will take only values of 1, 2, and index printed in *Latin letter* will take values of 1, 2, and 3. The partial derivatives of functions F with respect to surface coordinates $x^{\alpha}$ will be denoted by $F_{,\alpha}$.

The elements of differential geometry of the surfaces are developed in chapter 2, which is include the introducing the first fundamental form and second fundamental forms *changing of curvature tensor*. Particularly, the main concepts of surface vectors and spatial vectors are reviewed, together associated mathematical formulas from differential geometry. Chapter 3 begins with the introduction into the concepts of surface deformation from the point of mapping. The Euler-Lagrange deformation tensors of first kind and second kind are defined. Then deformation measure formulas as a function of displacement vector are described. Application of deformation measure tools on the real surface of the Earth expressed in chapter 4.A *Gaussian* representation of the Earth surface in terms of the geodetic coordinates with respect to the reference ellipsoid is assumed and invariants of *changing of metric tensor and changing of curvature tensor* are extracted. The efficiency of developed deterministic method for geometrical modelling of the Earth surface deformation is demonstrated in chapter 5 by analysis of data sets. The southern *California*, which is selected for the analysis of the capacities of the intrinsic method, is known as an extraordinary natural laboratory the study of geodynamics process. We investigated the links between various patterns of the surface deformation measure tools with geophysical and seismological evidence of the test area to judge the validity of our results. Chapter 6 concludes the main contribution and results in this study and makes a prospect of further applications of developed theory and methods conclude the study.

# Chapter 2

## Elements of Differential Geometry of a Surface

Differential geometry of a surface has been developed in details in many mathematical monographs. An excellent introduction to differential geometry of a surface, within the scope necessary in *shells theory* and *map projection*, may be found in the books of *E. Grafarend and Friedrich W. Krumm* (2006) , *A. Visconti* (1992), *D. Martin* (1991), *N. Prakash* (1981).Here we present an introduction to differential geometry of a surface and *Riemannian manifolds*. Thus, the basic definitions and principles of the theory of *manifolds*, within the scope necessary for this study, are recapitulated here. In fact, this chapter introduces the mathematical language of this thesis.

## 2-1. Geometry of a surface

An embedded *Riemann manifold* $\mathbb{M}^2$ in *3–dimensional Euclidean space* $\mathbb{E}^3$, namely *embedding space*, can be defined by three scalar functions of two parameters

$$\begin{aligned} & x^1 = f^1(\theta^1,\theta^2), x^2 = f^2(\theta^1,\theta^2), x^3 = f^3(\theta^1,\theta^2) \\ & \mathbf{x} = \overrightarrow{OM} = \mathbf{f}(\theta^1,\theta^2) = \sum_{k=1}^{3} \mathbf{j}_k \, f^k(\theta^1,\theta^2) = \mathbf{j}_k x^k \quad , \quad k \in \{1,2,3\} \end{aligned} \tag{2.1}$$

where the *summation convention* over the repeated index k has been used . The vector $\mathbf{x}$ is known as the position vector of the surface points $M \in \mathbb{M}^2$ while $x^k$ , $k \in \{1,2,3\}$ and $\theta^\alpha$ , $\alpha \in \{1,2\}$ are called *Cartesian* and *curvilinear Gaussian coordinates* of the *Riemann manifold*, respectively. In other words, a generic point in *Euclidean* space $\mathbb{E}^3$ can be a set of three coordinates while a generic point on the *Riemann manifold* $\mathbb{M}^2$ can be characterized by a set of two *Gaussian* surface coordinates $\theta^\alpha$ . *Latin* indices will refer to space coordinates while *Greek* indices will refer to surface coordinates. The partial derivatives of functions F with respect to surface coordinates $x^\alpha$ will be denoted by $F_{,\alpha}$ .The subscripts in this notation must be understood as indices, which are subject to the summation convention. The first partial derivatives of the vector $\mathbf{x}$ with respect to *Gaussian* coordinates, tangent to the *Riemann manifold* at point $M$ , are the so-called *tangential base vectors*.

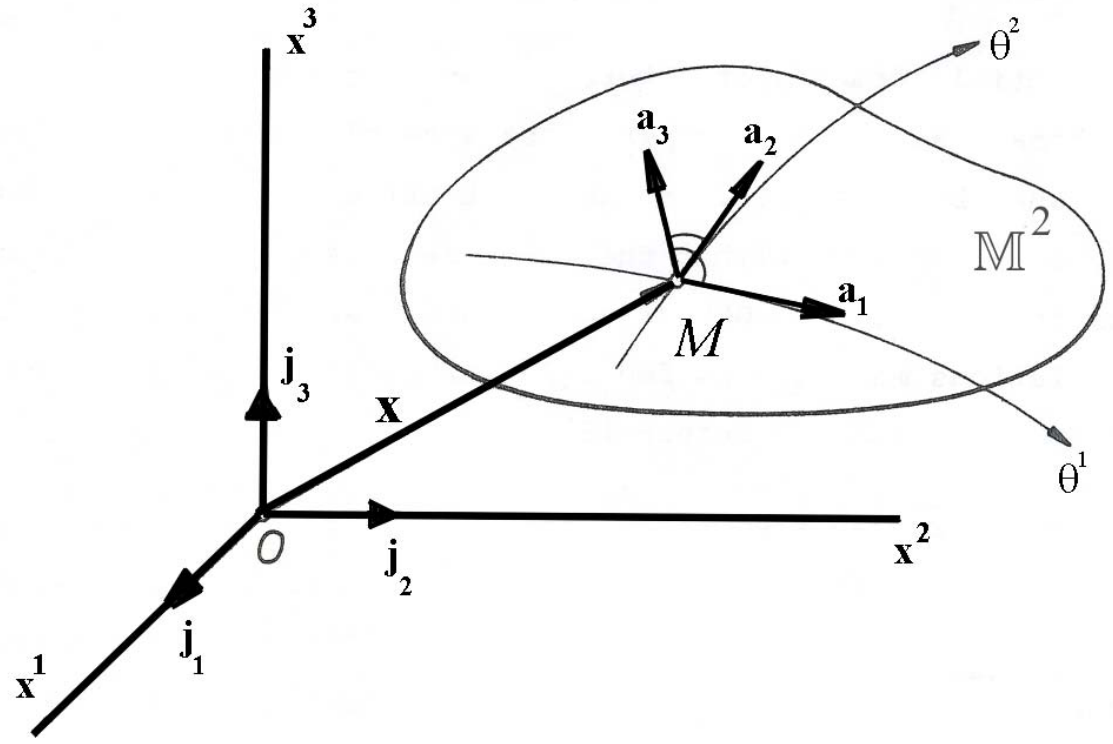


Fig 2-1: *Gaussian base vectors* $\{\mathbf{a}_1, \mathbf{a}_2, \mathbf{a}_3\}$

They characterized the directions of the curvilinear coordinates on the *Riemann manifold* $\mathbb{M}^2$ and defined by

Box 2-1 : *Gaussian base vectors*

$$\mathbf{a}_\alpha = \frac{\partial \mathbf{f}(\theta^\beta)}{\partial \theta^\alpha} \equiv \mathbf{x}_{,\alpha} = x^k{}_{,\alpha}\ \mathbf{j}_k$$
$$\mathbf{a}_3 = (\mathbf{a}_1 \times \mathbf{a}_2)/\left\|\mathbf{a}_1 \times \mathbf{a}_2\right\| \qquad (2.2)$$

where $\mathbf{a}_\alpha$ is the *covariant base vectors* of the two dimensional tangent vector space and × denotes vector product, which is taken according to the right-hand rule. The vector $\mathbf{a}_3$ called the unit normal vector to the *Riemann manifold*, since $<\mathbf{a}_3, \mathbf{a}_\alpha> = 0$ .The base vectors $\mathbf{a}_\alpha$ define at $M \in \mathbb{M}^2$ a two-dimensional linear vector space $\mathbb{V}$ in which we can introduce the *contravariant* base vectors $\mathbf{a}^\alpha$, dual to those of $\mathbf{a}_\alpha$ , by the relations $<\mathbf{a}_\alpha, \mathbf{a}^\beta> = \delta^\alpha_\beta$ where $\delta^\alpha_\beta$ is the *Kronecker* delta. In the other word, the vector $\mathbf{a}_\alpha$ is an element of the vector space $\mathbb{V}$, $\mathbf{a}^\alpha$ is an element of its dual space.

Meanwhile it is space of the linear functions over the elements of $\mathbb{V}$ [*Grafarend* 2004].It is easy to see that the vectors $\mathbf{a}^{\alpha}$ satisfying the equations $<\mathbf{a}_{\alpha},\mathbf{a}^{\beta}>=\delta_{\beta}^{\alpha}$ have the form

$$\mathbf{a}^{1}=\frac{\mathbf{a}_{2}\times\mathbf{a}_{3}}{<\mathbf{a}_{1}\times\mathbf{a}_{2},\mathbf{a}_{3}>} \qquad \textit{versus} \qquad \mathbf{a}^{2}=\frac{\mathbf{a}_{3}\times\mathbf{a}_{1}}{<\mathbf{a}_{1}\times\mathbf{a}_{2},\mathbf{a}_{3}>} \tag{2.3}$$

## 2-2. First fundamental form

The coefficients defined by $a_{\alpha\beta}=<\mathbf{a}_{\alpha},\mathbf{a}_{\beta}>=x^{k}{}_{,\alpha}x^{l}{}_{,\beta}\delta_{kl}$ are known as the *covariant components of the surface metric tensor* or *first fundamental form tensor of the surface*. The *contravariant* components $a^{\alpha\beta}$ of the *surface metric tensor* may be obtained from the following set of linear algebraic equations $a^{\alpha\beta}a_{\beta\gamma}=\delta_{\gamma}^{\alpha}$ .It follows now from the equations $<\mathbf{a}^{\alpha},\mathbf{a}_{\beta}>=\delta_{\beta}^{\alpha}$ and equations (2.3) that

$$\mathbf{a}^{\alpha}=a^{\alpha\beta}\mathbf{a}_{\beta} \;,\quad a^{\alpha\beta}=<\mathbf{a}^{\alpha},\mathbf{a}^{\beta}> \tag{2.4}$$

Indeed equation (2.4) transforms the *covariant* base vectors into the *contravariant* base vectors. These equations relate the *covariant* and *contravariant* basic vectors. It should be noted, that due to the normality of the unit normal vector and its orthogonality to the tangent base vectors the unit normal vector and its reciprocal vector are equal and consequently there is no difference between the *contravariant* and *covariant* coordinates of normal vector. In various geometrical formulae, it is convenient to make use of surface quantities: $\varepsilon_{\alpha\beta}=<\mathbf{a}_{\alpha}\times\mathbf{a}_{\beta},\mathbf{a}_{3}>$ *versus* $\varepsilon^{\alpha\beta}=<\mathbf{a}^{\alpha}\times\mathbf{a}^{\beta},\mathbf{a}_{3}>$ which are known as *covariant* and *contravariant* compoents of *surface alternation tensor* ,respectively. Using some algebraic transformations it is shown that [*Ernst* 1981]

$$\left[<\mathbf{a}_{1}\times\mathbf{a}_{2},\mathbf{a}_{3}>\right]^{2}=\begin{vmatrix}<\mathbf{a}_{1},\mathbf{a}_{1}> & <\mathbf{a}_{1},\mathbf{a}_{2}> & <\mathbf{a}_{1},\mathbf{a}_{3}>\\ <\mathbf{a}_{2},\mathbf{a}_{1}> & <\mathbf{a}_{2},\mathbf{a}_{2}> & <\mathbf{a}_{2},\mathbf{a}_{3}>\\ <\mathbf{a}_{3},\mathbf{a}_{1}> & <\mathbf{a}_{3},\mathbf{a}_{2}> & <\mathbf{a}_{3},\mathbf{a}_{3}>\end{vmatrix}=a>0 \tag{2.5}$$

and for alternative tensor components we obtain

$$\begin{aligned}\varepsilon_{12}&=-\varepsilon_{21}=\sqrt{a} \quad , \quad \varepsilon_{11}=\varepsilon_{22}=0\\ \varepsilon^{12}&=-\varepsilon^{21}=\frac{1}{\sqrt{a}} \quad , \quad \varepsilon^{11}=\varepsilon^{22}=0\end{aligned} \tag{2.6}$$

where

$$\begin{aligned} &\mathbf{a}_\alpha \times \mathbf{a}_\beta = \varepsilon_{\alpha\beta}\mathbf{a}_3 \quad , \quad \mathbf{a}^\alpha \times \mathbf{a}^\beta = \varepsilon^{\alpha\beta}\mathbf{a}_3 \\ &\mathbf{a}_3 \times \mathbf{a}_\alpha = \varepsilon_{\alpha\beta}\mathbf{a}^\beta \quad , \quad \mathbf{a}_3 \times \mathbf{a}^\alpha = \varepsilon^{\alpha\beta}\mathbf{a}_\beta \\ &\mathbf{a}_3 = \frac{1}{2}\varepsilon_{\alpha\beta}(\mathbf{a}_\alpha \times \mathbf{a}_\beta) = \frac{1}{2}\varepsilon_{\alpha\beta}(\mathbf{a}^\alpha \times \mathbf{a}^\beta) \end{aligned} \tag{2.7}$$

These formulae are very useful in general discussion of various geometrical relations at a *Riemann manifold*.

## 2-3. Second fundamental form

Differentiating the unit normal with respect to surface coordinates, we obtain two vectors tangent to the *Riemann manifold* at point $M$ , $\mathbf{a}_{3,\alpha} \in \mathbb{V}$ .The coefficients defined by

$$b_{\alpha\beta} = -<\mathbf{a}_{3,\alpha}, \mathbf{a}_\beta> = -<\mathbf{a}_{3,\beta}, \mathbf{a}_\alpha> = <\mathbf{a}_3, \mathbf{a}_{\alpha,\beta}> \tag{2.8}$$

where are known *covariant* components of *a surface curvature tensor* or *second fundamental form* .Having the *covariant* coordinates of the first fundamental tensor $a_{\alpha\beta}$ and the second fundamental tensor $b_{\alpha\beta}$ of the *Riemann manifold.* The components $b_{\alpha\beta}$ can also be given in terms of *Cartesian* components of the normal vector and the partial derivatives of the direction coefficients: $b_{\alpha\beta} = x^k{}_{,\alpha\beta}\, a_{3k}$ .*Gaussian curvature* K and *mean curvature* H can be determined as two geometric *invariants* associated with these tensors

$$\begin{aligned} K &= \frac{1}{2}\varepsilon^{\alpha\gamma}\varepsilon^{\beta\mu}b_{\alpha\beta}b_{\lambda\mu} = \frac{b}{a} \quad , b = \left|b_{\alpha\beta}\right| \\ H &= \frac{1}{2}a^{\alpha\beta}b_{\alpha\beta} \end{aligned} \tag{2.9}$$

## 2-4. Surface vectors

Any surface vector $\mathbf{v} \in \mathbb{V}$ may be represented by its components, *covariant bases* or *contravariant bases*, respectively, according to the linear relations

$$\mathbf{v} = v^\alpha \mathbf{a}_\alpha = v_\alpha \mathbf{a}^\alpha \qquad where \;:\; v^\alpha = <\mathbf{v}, \mathbf{a}^\alpha> \qquad versus \qquad v_\alpha = <\mathbf{v}, \mathbf{a}_\alpha> \tag{2.10}$$

where $v^\alpha$ and $v_\alpha$ are called *contravariant* and *covariant* components of surface vector $\mathbf{v}$, respectively. By means of the equation (2.4) we obtain

$$v^\alpha = a^{\alpha\beta} v_\beta \quad , \quad v_\alpha = a_{\alpha\beta} v^\beta \tag{2.11}$$

This established a law for raising and lowering of indices of the vector components. The geometrical meaning of these components is illustrated in the figure 2-2.

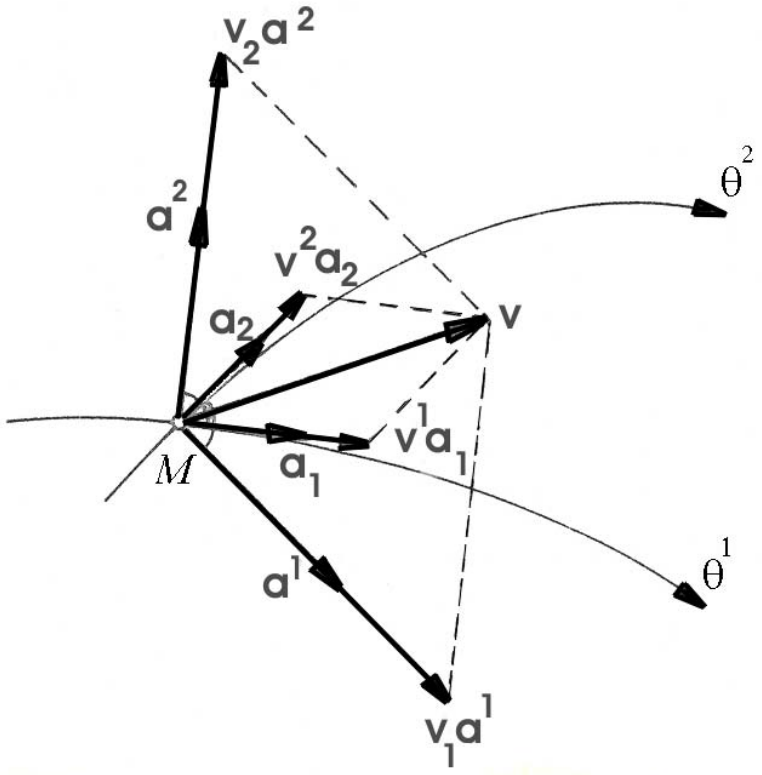


Fig 2-2: Illustration of surface vector components (*covariant, contravariant*)

## 2-41. Covariant differentiation

The partial derivatives of the tangential base vectors may be decompose with respect to the tangential base vectors themselves and the unit normal vector by means of *Gauss'* formula:

$$\mathbf{a}_{\alpha,\beta} = \mathbf{r}_{,\alpha\beta} = \Gamma^\kappa_{\alpha\beta} \mathbf{a}_\kappa + b_{\alpha\beta} \mathbf{a}_3 \tag{2.12}$$

The components $\Gamma^\kappa_{\alpha\beta}$ are called *surface Christoffel symbols* of the second kind, which is defined as vector components of the partial derivatives of the base vector $\mathbf{a}_\alpha$. They can be expressed in terms of the components of the metric tensor by means of

$$\Gamma^{\mu}_{\alpha\beta} = a^{\mu\gamma}\Gamma_{\alpha\beta\gamma} =< \mathbf{a}^{\mu}, \mathbf{a}_{\alpha,\beta} >= - < \mathbf{a}^{\mu}{}_{,\alpha}, \mathbf{a}^{\beta} >$$
$$\Gamma_{\alpha\beta\gamma} = \frac{1}{2}(a_{\beta\gamma,\alpha} + a_{\gamma\alpha,\beta} - a_{\alpha\beta,\gamma}) \qquad (2.13)$$

The components $\Gamma_{\alpha\beta\gamma}$ are called *surface Christoffel symbols of the first kind.* Let us differentiate a surface vector field $\mathbf{v} \in \mathbb{V}$ along the coordinate lines

Box 2-2 *: Differentiate a surface vector w.r.t surface coordinates*

$$\mathbf{v}_{,\beta} = \frac{\partial}{\partial\theta^{\beta}}(v^{\alpha}\mathbf{a}_{\alpha}) = (v^{\alpha}{}_{,\beta} + \Gamma^{\alpha}_{\lambda\beta}v^{\lambda})\mathbf{a}_{\alpha} + b_{\alpha\beta}v^{\alpha}\mathbf{a}_3$$
$$= v^{\alpha}\,|_{\beta}\,\mathbf{a}_{\alpha} + b_{\alpha\beta}v^{\alpha}\mathbf{a}_3 = v_{\alpha|\beta}\mathbf{a}^{\beta} + b^{\alpha}_{\beta}v_{\alpha}\mathbf{a}_3 \qquad (2.14)$$

where operations defined by

$$v^{\alpha}\,|_{\beta} = v^{\alpha}{}_{,\beta} + \Gamma^{\alpha}_{\lambda\beta}v^{\lambda} \quad \textit{versus} \quad v_{\alpha|\beta} = v_{\alpha,\beta} - \Gamma^{\lambda}_{\alpha\beta}v_{\lambda} \qquad (2.15)$$

are called the *covariant derivative* of the surface vector components.

## 2-5. Spatial vectors

We shall have to deal with *spatial vectors* $\mathbf{u} \in \mathbb{U} \equiv \mathbb{V} \times \mathbb{N}$, where $\mathbb{N}$ is a one-dimensional vector space, orthogonal to $\mathbb{V}$ , having the unit normal vector $\mathbf{a}_3$ as its basis, and $\times$ in here is the *Cartesian* product operation. The spatial vector $\mathbf{u}$ is expressible in terms of its components in the spatial basis $\mathbf{a}_k$ , $k = \{1,2,3\}$ or $\mathbf{a}^k$ according to

Box 2-3 : *Differentiate spatial vector w.r.t surface coordinates*

$$\mathbf{u} = u^{\alpha}\mathbf{a}_{\alpha} + u^3\mathbf{a}_3 \qquad (2.16)$$

and using (2.14) we obtain

$$\mathbf{u}_{,\beta} = (u^{\alpha}\,|_{\beta} - b^{\alpha}_{\beta}u^3)\mathbf{a}_{\alpha} + (u^3{}_{,\beta} + b_{\alpha\beta}u^{\alpha})\mathbf{a}_3$$
$$= (u_{\alpha|\beta} - b_{\alpha\beta}u^3)\mathbf{a}^{\alpha} + (u^3{}_{,\beta} + b^{\alpha}_{\beta}u_{\alpha})\mathbf{a}_3 \qquad (2.17)$$

# Chapter 3

# Deformation of the Surface

By surface deformation, we understood a one-to-one mapping from one *Riemann manifold*, namely *left*, on another *Riemann manifold*, namely *right*. In shells theory literatures left one is called *reference* or un-deformed surface while the right one is called the *current* or *deformed* surface. In terms of the geometry of surfaces, this is taking reference to its *first fundamental form*, and *second fundamental form*. In particular, in order to derive certain invariant measure of such mapping, namely deformation measures, a *canonical formalism* is applied: The simultaneous diagonalization of two symmetry matrices is of focal interest. Such diagonalization is in the following form

*Simultaneous diagonalization of two symmetric matrices* :

*If* $A \in \mathbb{R}^{n\times n}$ *is a symmetric matrix and* $B \in \mathbb{R}^{n\times n}$ *is a symmetric positive-definite matrix such that* $AB^{-1}$ *exists, then there exists a non-singular matrix* $X$ *such that both* $X^T AX = diag(\lambda_1, \lambda_2, \ldots, \lambda_n)$ *and* $X^T BX = I_n = diag(1,1,\ldots 1)$ *are diagonal matrices, namely* $I_n$ *the* $n$ *dimensional unit matrix.*

## 3-1. Mapping from the left to the right two dimensional Riemann manifold

Let there be given the *left* two–dimensional *Riemann manifold* $\left\{\mathbb{M}_l^2, G_{MN}\right\}$ and the *right* two–dimensional *Riemann manifold* $\left\{\mathbb{M}_r^2, g_{\mu\nu}\right\}$ with standard metric $\left[G_{MN}\right] = \left[G_{NM}\right]$ and $\left[g_{\mu\nu}\right] = \left[g_{\nu\mu}\right]$, respectively, both *symmetric* and *positive-definite*. An open subset $U_l \subset \mathbb{M}_l^2$ and $U_r \subset \mathbb{M}_r^2$ respectively, is covered by chart $\left\{\Phi_l, U_l\right\}$ and $\left\{\Phi_r, U_r\right\}$ respectively. Such charts are constituted by *surface* coordinates $\left\{\theta_l^1, \theta_l^2\right\} \in \Phi_l \subset \mathbb{R}^2$ and $\left\{\theta_r^1, \theta_r^2\right\} \in \Phi_r \subset \mathbb{R}^2$ over the open sets $\Phi(U_l)$ and $\Phi(U_r)$, respectively. Figure 3-1 illustrates by a *commutative diagram* the mapping $\overline{f} : \mathbb{M}_l^2 \to \mathbb{M}_r^2$ and $\underline{f} : \Phi(U_l) \to \Phi(U_r) = \Phi_r \circ \overline{f} \circ \Phi_l^{-1}$, which governs the descriptive elements once we transform from the *left Riemann manifold* to the *right Riemann manifold*, [*E. Grafarend and Friedrich W. Krumm* (2006)].

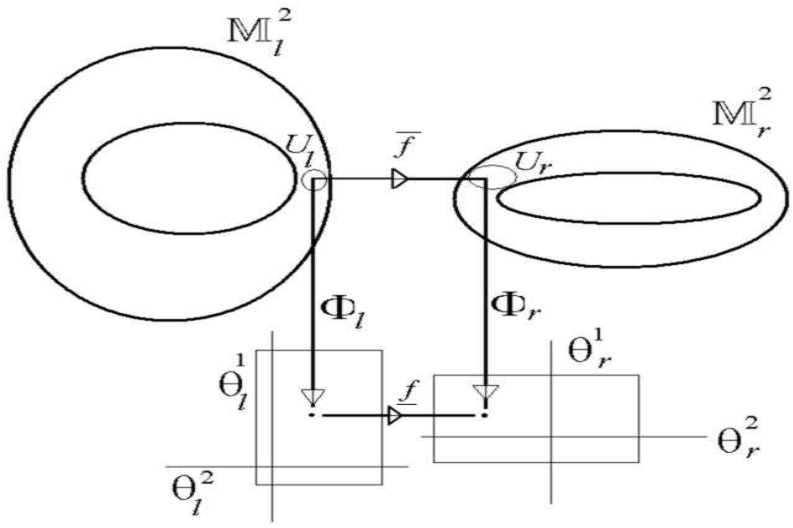


Fig 3-1: *The commutative diagram* $(\overline{f}, \underline{f}, \Phi_l, \Phi_r)$

## 3-2. Deformed surface geometry

The different ways of describing deformation may be used in general: *Lagrangian* or *Eulerian*. In the *Lagrangian* description, geometry of reference surface, or *left Riemann manifold*, is supposed to be known and all geometric quantities of *current* surface, or *right Riemann manifold*, are expressed in terms of geometric quantities of the *reference* surface and *displacement vector* between these two surfaces. In the *Eulerian*, description geometry of the *reference* surface is expressed in terms of *current* surface geometry and *displacements*. In this study we assumed geometry of reference surface is known and deformation of the surface are treated in *Lagrangian* portray. A comparative analysis of the *metric* tensors of the two manifolds under comparison is the standard way from the description of deformation in *continuum mechanics* [*A.C. Eringen* (1962), *G. Beda et al*. (1995), p.18; *D. B. Macvean* (1968), p.158]. A comprehensive review of various local as well as global multiplicative and additive measures of surface deformation, based on the *metric tensors* of two parameterized surfaces, is given in [*E. Grafarend and Friedrich W. Krumm* (2006)]. In addition to the metric tensor, a comprehensive analysis of the *second fundamental tensors* of the *reference* and *current* surface is

considered as a way of describing surface deformation in *shell theory*. In this study, we concentrate on the most common measures of surface deformation, which are derived from the *first and second fundamental tensors* of the two surfaces and some certain invariants of these derived measures.

## 3-21. A first multiplication measure of deformation: The Cauchy –Green deformation tensor

We recall the assumption that the *reference* and *current* surface are considered as 2-dimensional *Riemann manifolds* $\mathbb{M}_l^2$ and $\mathbb{M}_r^2$ embedded in 3-dimensional *Euclidean* spaces $\mathbb{E}^3$. The motion of 2-dimensional manifold carries various *reference* surface points through various *current* surface points. On the *reference* surface, the place in the embedding space of a generic point is given by the placement vector $\mathbf{X}$. After deformation, the place in space of the same point is given by a new placement vector $\mathbf{x}$. This is expressed by

$$\theta^\lambda = \theta^\lambda(\Theta^\Omega) \quad versus \quad \Theta^\Omega = \Theta^\Omega(\theta^\lambda) \tag{3.1}$$

which $\{\Theta^1, \Theta^2\}$ and $\{\theta^1, \theta^2\}$ are *surface convected coordinates* of *reference* surface and *current* surface . Then each point $m$ in the current surface comes from a point $M$ in *reference* surface, which is illustrated in figure 3-2. We assume the mapping are single valued and have continuous partial derivatives with respect to their arguments. Moreover, each member of this mapping is the unique inverse of the other in a neighbourhood of the reference surface point $M$ .A unique inverse of the first of (3.1) exists, at least in a $\delta$ neighbourhood of $m$ ,if and only if the determinant of *Jacobian* matrix is not identically zero,i.e., $\left|\partial\theta^\lambda / \partial\Theta^\Omega\right| \neq 0$ and $\left|\theta^\lambda - \theta_0^\lambda\right| < \delta$ . No region of positive, finite volume is deformed into one of zero or infinite volume. Referring to Figure 3-2, the displacement vector $\mathbf{u}$ is defined as $\mathbf{u} = \mathbf{X}(\Theta^1, \Theta^2) - \mathbf{x}(\theta^1, \theta^2)$ . Infinitesimal vectors $d\Theta$ in $\mathbb{M}_l$ and $d\theta$ in $\mathbb{M}_r$ may be expressed as

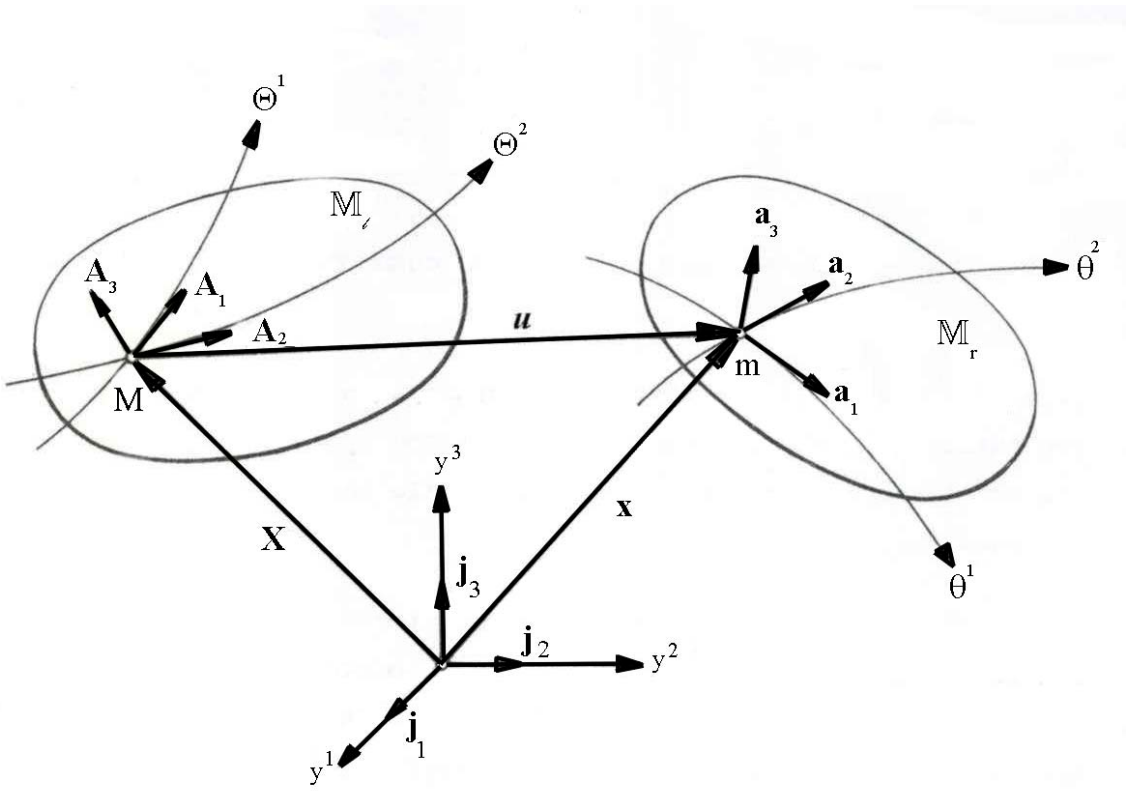


Fig 3-2: The *reference* and *current* surface

$$d\mathbf{X} = \frac{\partial \mathbf{X}}{\partial \Theta^{\Omega}} d\Theta^{\Omega} \qquad \textit{versus} \qquad d\mathbf{x} = \frac{\partial \mathbf{x}}{\partial \theta^{\lambda}} d\theta^{\lambda}$$
$$\mathbf{A}_{\Omega} = \frac{\partial \mathbf{X}}{\partial \Theta^{\Omega}} \qquad \textit{versus} \qquad \mathbf{a}_{\lambda} = \frac{\partial \mathbf{x}}{\partial \theta^{\lambda}} \tag{3.2}$$

where $\mathbf{A}_{\Omega}$ and $\mathbf{a}_{\lambda}$ are base vectors at $\Theta^{\Omega}$ and $\theta^{\Omega}$ ,respectively. The base vectors are tangential to the coordinate curve $\left\{\Theta^1, \Theta^2\right\}$ and $\left\{\theta^1, \theta^2\right\}$ .The tangential base vectors in *current* surface $\mathbf{a}_{\lambda}$ can be decomposed with respect to the tangential base vectors $\mathbf{A}_{\Omega}$ and the unit normal vector $\mathbf{A}_3$ in *reference* surface [*Ernst* 1981]

$$\mathbf{a}_{\lambda} = \ell^{\alpha}_{\bullet\lambda}\mathbf{A}_{\alpha} + \zeta_{\lambda}\mathbf{A}_3 \tag{3.3}$$

The components of the surface tensor $\ell^{\alpha}_{\bullet\lambda}$ and the surface vector $\zeta_{\lambda}$ can be given in terms of surface components of surface displacement vector

$$\zeta_{\lambda} = \tilde{U}^3_{,\lambda} + B^{\alpha}_{\lambda}\tilde{U}_{\alpha} = \tilde{U}^3_{,\lambda} + B_{\lambda\gamma}\tilde{U}^{\gamma}$$
$$\ell^{\alpha}_{\bullet\lambda} = \delta^{\alpha}_{\lambda} + \tilde{U}^{\alpha}\,|_{\lambda} - B^{\alpha}_{\lambda}\tilde{U}^3 \tag{3.4}$$

where coordinates of the mixed tensor $B_{\lambda}^{\alpha}$ can be obtained by the rule of raising indices applied to the tensor of second fundamental form $B_{\lambda\varsigma}$ as

$$B_{\lambda}^{\alpha} =< \mathbf{A}^{\alpha}, \mathbf{A}^{\varsigma} > B_{\lambda\varsigma} = A^{\alpha\varsigma} B_{\lambda\varsigma} \tag{3.5}$$

Then the unit normal vector to the *current* surface $\mathbf{a}_3$ can be expresses with respect to the tangential base vectors $\mathbf{A}_{\Omega}$ and the unit normal vector in *reference* surface $\mathbf{A}_3$

$$\mathbf{a}_3 = \frac{(\mathbf{a}_{\lambda} \times \mathbf{a}_{\tau})}{\|\mathbf{a}_{\lambda} \times \mathbf{a}_{\tau}\|} = \frac{(\ell_{\bullet\lambda}^{\alpha} \mathbf{A}_{\Omega} + \zeta_{\lambda} \mathbf{A}_3) \times (\ell_{\bullet\tau}^{\beta} \mathbf{A}_{\Psi} + \zeta_{\tau} \mathbf{A}_3)}{\left\|\ell_{\bullet\lambda}^{\alpha} \mathbf{A}_{\Omega} + \zeta_{\lambda} \mathbf{A}_3) \times (\ell_{\bullet\tau}^{\beta} \mathbf{A}_{\Psi} + \zeta_{\tau} \mathbf{A}_3\right\|} \tag{3.6}$$

Assuming the two, *Riemann manifolds* $\{\mathbb{M}_l, A_{\Omega\Phi}\}$ and $\{\mathbb{M}_r, a_{\lambda\phi}\}$ as embedded submanifolds of two different *3-dimensional Euclidean spaces* $\mathbb{E}^3$, the *first fundamental forms* $I_l$ of the $\mathbb{M}_l$ and the *first fundamental forms* $I_r$ of the $\mathbb{M}_r$ in surface local coordinates of manifolds are specified by

Box 3-1 *: Left versus right Cauchy-Green deformation tensor*

$I_l =< d\mathbf{X}, d\mathbf{X} >= A_{\Omega\Phi}(\Theta^{\Psi}) d\Theta^{\Omega} d\Theta^{\Phi}$ *versus* $I_r =< d\mathbf{x}, d\mathbf{x} >= a_{\lambda\phi}(\theta^{\psi}) d\theta^{\lambda} d\theta^{\phi}$

*Lagrangian first fundamental form*

$$I_l = A_{\Omega\Phi}(\Theta^{\Psi}) d\Theta^{\Omega} d\Theta^{\Phi}$$
$$= A_{\Omega\Phi}(\Theta^{\Psi}) \frac{\partial \Theta^{\Omega}}{\partial \theta^{\lambda}} \frac{\partial \Theta^{\Phi}}{\partial \theta^{\phi}} d\theta^{\lambda} d\theta^{\phi}$$
$$= A_{\Omega\Phi}(\Theta^{\Psi}) \Theta^{\Omega}{}_{,\lambda} \Theta^{\Phi}{}_{,\phi} d\theta^{\lambda} d\theta^{\phi}$$

*Eulerian first fundamental form*

$$I_r = a_{\lambda\phi}(\theta^{\psi}) d\theta^{\lambda} d\theta^{\phi}$$
$$= a_{\lambda\phi}(\theta^{\psi}) \frac{\partial \theta^{\lambda}}{\partial \Theta^{\Omega}} \frac{\partial \theta^{\phi}}{\partial \Theta^{\Phi}} d\Theta^{\Omega} d\Theta^{\Phi}$$
$$= a_{\lambda\phi}(\theta^{\psi}) \theta^{\lambda}{}_{,\Omega} \theta^{\phi}{}_{,\Phi} d\Theta^{\Omega} d\Theta^{\Phi}$$

*Left Cauchy - Green deformation tensor*

$$I_l = c_{\lambda\phi}(\theta^{\psi}) d\theta^{\lambda} d\theta^{\phi}$$

*where*

$$c_{\lambda\phi}(\theta^{\psi}) = A_{\Omega\Phi}(\Theta^{\Psi}) \Theta^{\Omega}{}_{,\lambda} \Theta^{\Phi}{}_{,\phi}$$

*Right Cauchy - Green deformation tensor*

$$I_r = C_{\Omega\Phi}(\Theta^{\Psi}) d\Theta^{\Omega} d\Theta^{\Phi}$$

*where*

$$C_{\Omega\Phi}(\Theta^{\Psi}) = a_{\lambda\phi}(\theta^{\psi}) \theta^{\lambda}{}_{,\Omega} \theta^{\phi}{}_{,\Phi} \tag{3.7}$$

which $c_{\lambda\phi}$ and $C_{\Omega\Phi}$ are called *left Cauchy-Green deformation tensor* and *right Cauchy-Green deformation tensor*, respectively. Both of these tensors are *symmetrical* and *positive-definite*.

## 3-22. Strain tensor

The difference of the *first fundamental form* of *reference* surface and *current* surface lead us to the definition of well-known additive measure of deformation called *Euler-Lagrange deformation tensor of first kind* or *tensor of change of metric*. The *symmetric Euler-Lagrange deformation tensors* are symmetric and play power tools in studying deformation.

Box 3-2 : *Left versus right Euler-Lagrange deformation tensors*

$$
\begin{aligned}
I_r - I_l &= a_{\lambda\phi} d\theta^\lambda d\theta^\phi - A_{\Omega\Phi} d\Theta^\Omega d\Theta^\Phi \\
&= (a_{\lambda\phi} \frac{d\theta^\lambda}{d\Theta^\Omega} \frac{d\theta^\phi}{d\Theta^\Phi} - A_{\Omega\Phi}) d\Theta^\Omega d\Theta^\Phi \\
&= (C_{\Omega\Phi} - A_{\Omega\Phi}) d\Theta^\Omega d\Theta^\Phi \\
&= 2E_{\Omega\Phi} d\Theta^\Omega d\Theta^\Phi
\end{aligned}
\qquad
\begin{aligned}
I_r - I_l &= a_{\lambda\phi} d\theta^\lambda d\theta^\phi - A_{\Omega\Phi} d\Theta^\Omega d\Theta^\Phi \\
&= (a_{\lambda\phi} - A_{\Omega\Phi} \frac{d\Theta^\Omega}{d\theta^\lambda} \frac{d\Theta^\Phi}{d\theta^\phi}) d\theta^\lambda d\theta^\phi \\
&= (a_{\lambda\phi} - c_{\lambda\phi}) d\theta^\lambda d\theta^\phi \\
&= 2e_{\lambda\phi} d\theta^\lambda d\theta^\phi
\end{aligned}
\qquad (3.8)
$$

*where*

$$
\begin{aligned}
E_{\Omega\Phi} &= \frac{1}{2}(a_{\lambda\phi} \frac{d\theta^\lambda}{d\Theta^\Omega} \frac{d\theta^\phi}{d\Theta^\Phi} - A_{\Omega\Phi}) \\
&= \frac{1}{2}(C_{\Omega\Phi} - A_{\Omega\Phi})
\end{aligned}
\qquad
\begin{aligned}
e_{\lambda\phi} &= \frac{1}{2}(a_{\lambda\phi} - A_{\Omega\Phi} \frac{d\Theta^\Omega}{d\theta^\lambda} \frac{d\Theta^\Phi}{d\theta^\phi}) \\
&= \frac{1}{2}(a_{\lambda\phi} - c_{\lambda\phi})
\end{aligned}
$$

## 3-23. Changing of curvature tensor

In surface deformation analysis, as another additive measure of surface deformation we can take into account the difference between the *second fundamental forms* of the surface at the *reference*- and *current* state. The additive comparison of the *second fundamental form* leads us to the definition of the *Euler-Lagrange deformation tensor of the second kind* or the *tensor of change of curvature*.

Box 3-3 *: Left versus right Euler-Lagrange deformation tensors of second type*

$$
\begin{aligned}
II_r - II_l &= b_{\lambda\phi} d\theta^\lambda d\theta^\phi - B_{\Omega\Phi} d\Theta^\Omega d\Theta^\Phi \\
&= (b_{\lambda\phi} \frac{d\theta^\lambda}{d\Theta^\Omega} \frac{d\theta^\phi}{d\Theta^\Phi} - B_{\Omega\Phi}) d\Theta^\Omega d\Theta^\Phi \\
&= K_{\Omega\Phi} d\Theta^\Omega d\Theta^\Phi
\end{aligned}
\qquad
\begin{aligned}
II_r - II_l &= b_{\lambda\phi} d\theta^\lambda d\theta^\phi - B_{\Omega\Phi} d\Theta^\Omega d\Theta^\Phi \\
&= (b_{\lambda\phi} - B_{\Omega\Phi} \frac{d\Theta^\Omega}{d\theta^\lambda} \frac{d\Theta^\Phi}{d\theta^\phi}) d\theta^\lambda d\theta^\phi \\
&= k_{\lambda\phi} d\theta^\lambda d\theta^\phi
\end{aligned}
\qquad (3.9)
$$

*where*

$$
K_{\Omega\Phi} = b_{\lambda\phi} \frac{d\theta^\lambda}{d\Theta^\Omega} \frac{d\theta^\phi}{d\Theta^\Phi} - B_{\Omega\Phi}
\qquad
k_{\lambda\phi} = b_{\lambda\phi} - B_{\Omega\Phi} \frac{d\Theta^\Omega}{d\theta^\lambda} \frac{d\Theta^\Phi}{d\theta^\phi}
$$

## 3-3. Deformation measurement tools as a function of displacement vector

For the practical application of the theory, it is more convenient that measures of deformation be expressed as a function of displacement vector $\mathbf{u}$.Thus we developed the measurement tools as a function of displacement vector and considered nonlinear terms of these relations. By means of *chain rule* and equation (3.8)

Box 3-4 *: Left versus right Cauchy-Green deformation tensors as a function of displacement vector* $\mathbf{u}$

$$
\begin{aligned}
C_{\Omega\Phi}(\Theta^{\Psi}) &= a_{\lambda\phi}(\theta^{\psi})\theta^{\lambda}{}_{,\Omega}\theta^{\phi}{}_{,\Phi} & c_{\lambda\phi}(\theta^{\psi}) &= A_{\Omega\Phi}(\Theta^{\Psi})\Theta^{\Omega}{}_{,\lambda}\Theta^{\Phi}{}_{,\phi} \\
&=< \frac{\partial \mathbf{x}}{\partial \Theta^{\Omega}}, \frac{\partial \mathbf{x}}{\partial \Theta^{\Phi}} > & &=< \frac{\partial \mathbf{X}}{\partial \theta^{\lambda}}, \frac{\partial \mathbf{X}}{\partial \theta^{\phi}} > \\
&=< \frac{\partial(\mathbf{u}+\mathbf{X})}{\partial \Theta^{\Omega}}, \frac{\partial(\mathbf{u}+\mathbf{X})}{\partial \Theta^{\Phi}} > & &=< \frac{\partial(\mathbf{x}-\mathbf{u})}{\partial \theta^{\lambda}}, \frac{\partial(\mathbf{x}-\mathbf{u})}{\partial \theta^{\phi}} > \\
&=< \frac{\partial \mathbf{u}}{\partial \Theta^{\Omega}}, \frac{\partial \mathbf{u}}{\partial \Theta^{\Phi}} > + < \frac{\partial \mathbf{u}}{\partial \Theta^{\Omega}}, \frac{\partial \mathbf{X}}{\partial \Theta^{\Phi}} > + & &=< \frac{\partial \mathbf{x}}{\partial \theta^{\lambda}}, \frac{\partial \mathbf{x}}{\partial \theta^{\phi}} > + < \frac{\partial \mathbf{u}}{\partial \theta^{\lambda}}, \frac{\partial \mathbf{u}}{\partial \theta^{\phi}} > - \quad (3.10) \\
&< \frac{\partial \mathbf{X}}{\partial \Theta^{\Omega}}, \frac{\partial \mathbf{u}}{\partial \Theta^{\Phi}} > + < \frac{\partial \mathbf{X}}{\partial \Theta^{\Omega}}, \frac{\partial \mathbf{X}}{\partial \Theta^{\Phi}} > & &=< \frac{\partial \mathbf{x}}{\partial \theta^{\lambda}}, \frac{\partial \mathbf{u}}{\partial \theta^{\phi}} > - < \frac{\partial \mathbf{u}}{\partial \theta^{\lambda}}, \frac{\partial \mathbf{x}}{\partial \theta^{\phi}} > \\
&=< \mathbf{u}_{,\Omega}\ ,\ \mathbf{u}_{,\Phi} > + < \mathbf{u}_{,\Omega}\ ,\ \mathbf{A}_{\Phi} > + & &=< \mathbf{a}_{\lambda}\ ,\mathbf{a}_{\phi} > + < \mathbf{u}_{,\lambda}\ ,\mathbf{u}_{,\phi} > - \\
&< \mathbf{A}_{\Omega}\ ,\ \mathbf{u}_{,\Phi} > + < \mathbf{A}_{\Omega}\ ,\ \mathbf{A}_{\Phi} > & &< \mathbf{a}_{\lambda}\ ,\mathbf{u}_{,\phi} > - < \mathbf{u}_{,\lambda}\ ,\mathbf{a}_{\phi} >
\end{aligned}
$$

Analogous to the left and right *Cauchy-Green* deformation tensor as a function of displacement vector, we can derive left and right *Euler-Lagrange* deformation tensor as a function of displacement vector by subtracting of metric tensor and *Cauchy-Green* deformation tensor

Box 3-5 : *Left versus Euler-Lagrange deformation tensors of the first kind as a function of displacement vector* $\mathbf{u}$

$$
\begin{aligned}
E_{\Omega\Phi} &= \frac{1}{2}(C_{\Omega\Phi} - A_{\Omega\Phi}) & e_{\lambda\phi} &= \frac{1}{2}(a_{\lambda\phi} - c_{\lambda\phi}) \\
&= \frac{1}{2}(< \mathbf{u}_{,\Omega}\ ,\ \mathbf{u}_{,\Phi} > + < \mathbf{u}_{,\Omega}\ ,\ \mathbf{A}_{\Phi} > + & &= \frac{1}{2}(< \mathbf{u}_{,\lambda}\ ,\mathbf{u}_{,\phi} > - < \mathbf{a}_{\lambda}\ ,\mathbf{u}_{,\phi} > - \quad (3.11) \\
&< \mathbf{A}_{\Omega}\ ,\ \mathbf{u}_{,\Phi} >) & &< \mathbf{u}_{,\lambda}\ ,\mathbf{a}_{\phi} >)
\end{aligned}
$$

In analogy to the *Euler-Lagrange deformation tensor of the first kind*, it is suitable to have the *Lagrangian deformation tensors of the second kind* or the *tensor of change of curvature* as functions of the displacement vector. To overcome this problem we use the difference between the normal vectors in the *reference* surface $\mathbf{A}_3$ and the normal vectors in the *current* surface $\mathbf{a}_3$ which $\mathbf{w} = \mathbf{a}_3 - \mathbf{A}_3$ [*Stein* 1980]. Box (3.6) introduces the coordinates of the *Euler-Lagrange deformation*

*tensor of the second kind*. As it can be seen in this box, we end up with expressions of the *Euler-Lagrange deformation tensor of second type* as inner products of the partial derivatives of spatial vectors **w** and **u**, relative to curvilinear coordinates and tangent base vectors.

Box 3-6 : *Left versus right Euler-Lagrange deformation tensor of second type as a function of displacement vector* **u**

$$K_{\Omega\Phi} = b_{\lambda\phi}\frac{d\theta^{\lambda}}{d\Theta^{\Omega}}\frac{d\theta^{\phi}}{d\Theta^{\Phi}} - B_{\Omega\Phi} = -\frac{d\theta^{\lambda}}{d\Theta^{\Omega}}\frac{d\theta^{\phi}}{d\Theta^{\Phi}} < \frac{\partial \mathbf{a}_3}{\partial\theta^{\lambda}}, \mathbf{a}_{\phi} > -B_{\Omega\Phi}$$

$$= -\frac{d\theta^{\lambda}}{d\Theta^{\Omega}}\frac{d\theta^{\phi}}{d\Theta^{\Phi}} < \frac{\partial(\mathbf{w}+\mathbf{A}_3)}{\partial\theta^{\lambda}}, \frac{\partial(\mathbf{X}+\mathbf{u})}{d\theta^{\phi}} > -B_{\Omega\Phi}$$

$$= - < \mathbf{w}_{,\Omega}, \mathbf{A}_{\Phi} > - < \mathbf{w}_{,\Omega}, \mathbf{u}_{,\Phi} > - < \mathbf{A}_{3,\Omega}, \mathbf{u}_{,\Phi} >$$

*where*

$$\mathbf{A}_{3,\Omega} = -B_{\Omega\Psi}\mathbf{A}^{\Psi}$$

*versus*

$$k_{\lambda\phi} = b_{\lambda\phi} - B_{\Omega\Phi}\frac{d\Theta^{\Omega}}{d\theta^{\lambda}}\frac{d\Theta^{\Phi}}{d\theta^{\phi}} = b_{\lambda\phi} + \frac{d\Theta^{\Omega}}{d\theta^{\lambda}}\frac{d\Theta^{\Phi}}{d\theta^{\phi}} < \frac{\partial \mathbf{A}_3}{\partial\Theta^{\Omega}}, \mathbf{A}_{\Phi} >$$

$$= b_{\lambda\phi} - \frac{d\Theta^{\Omega}}{d\theta^{\lambda}}\frac{d\Theta^{\Phi}}{d\theta^{\phi}} < \frac{\partial(\mathbf{w}-\mathbf{a}_3)}{\partial\Theta^{\Omega}}, \frac{\partial(\mathbf{x}-\mathbf{u})}{\partial\Theta^{\Omega}} >$$

$$= - < \mathbf{w}_{\lambda}, \mathbf{a}_{\phi} > + < \mathbf{w}_{\lambda}, \mathbf{u}_{,\phi} > - < \mathbf{a}_{3,\lambda}, \mathbf{u}_{,\phi} >$$

*where*

$$\mathbf{a}_{3,\lambda} = -b_{\lambda\psi}\mathbf{a}^{\psi} \qquad (3.12)$$

# Chapter 4

## The Earth Surface Deformation

The typical problem we are confronted with it is of the following type. We use surface coordinates $\{\Lambda,\Phi\}$, called ellipsoidal longitude and latitude, by which we intend to describe a point on the *Earth's surface*, which is given in a *3-dimensional Euclidean space* $\mathbb{E}^3$ or embedding space $\{X,Y,Z\}$. By means of the ambient space, which is represented in terms of given functions $\{X(\Lambda,\Phi,\tilde{H}(\Lambda,\Phi)),Y(\Lambda,\Phi,\tilde{H}(\Lambda,\Phi)),Z(\Lambda,\Phi,\tilde{H}(\Lambda,\Phi))\}$ and known *''height functions''* $\tilde{H}(\Lambda,\Phi)$, in terms of geodetic coordinates we arrive with the *Gauss surface coordinate representation* [*Grafarend et al*., 1992].

$$\mathbf{X}(\Lambda,\Phi)=\mathbf{j}_1 X^1(\Lambda,\Phi)+\mathbf{j}_2 X^2(\Lambda,\Phi)+\mathbf{j}_3 X^3(\Lambda,\Phi)$$

$$\mathbf{X}(\Lambda,\Phi)=\begin{bmatrix}\mathbf{j}_1 & \mathbf{j}_2 & \mathbf{j}_3\end{bmatrix}\begin{bmatrix}\dfrac{A}{\sqrt{1-E^2\sin^2\Phi}}+\tilde{H}(\Lambda,\Phi)\\ \dfrac{A}{\sqrt{1-E^2\sin^2\Phi}}+\tilde{H}(\Lambda,\Phi)\\ \dfrac{A(1-E^2)}{\sqrt{1-E^2\sin^2\Phi}}+\tilde{H}(\Lambda,\Phi)\end{bmatrix}\begin{bmatrix}\cos(\Lambda)\cos(\Phi) & \sin(\Lambda)\cos(\Phi) & \sin(\Phi)\end{bmatrix} \tag{4.1}$$

With respect to the *International Reference Ellipsoid*, we call: A as a semi-major axis, B as semi-minor axis, $E^2=(A^2-B^2)/A^2$ is the square of first relative eccentricity. Placement vector $\mathbf{X}(\Lambda,\Phi)$ in the *reference* state, in equation(4.1), is expressed by *orthonormal fixed frames* $\{\mathbf{j}_1,\mathbf{j}_2,\mathbf{j}_3\}$.In the *intrinsic approach*, we consider three base vectors to be associated to any point on the reference surface and current surface namely, the unit normal vector and two tangent base vectors along the surface components, which are illustrated in chapter 2. It plays an essential role in deformation analysis of surfaces based on the *intrinsic approach* and called *Gaussian surface moving frame*. The tangent bases vectors are derived by partial derivatives of *Gaussian* representation of the Earth's surface relative to surface curvilinear coordinates and the unit normal vector at the point p on the *reference* surface with respect to the surface curvilinear coordinates $(\Lambda,\Phi)$ will be obtained by equations (2.2) in chapter 2. The base vectors of the two dimensional tangent vector space are

constructed by $\mathbf{A}_1 = \partial \mathbf{X}(\Lambda,\Phi)/\partial\Theta^1$ and $\mathbf{A}_2 = \partial \mathbf{X}(\Lambda,\Phi)/\partial\Theta^2$. The surface curvilinear coordinates of the displacement vector, *covariant* or *contravariant*, can be obtained as the inner product of space coordinates of the displacement vector **u** and surface base vectors by the following way: $\tilde{U}_\Omega = <\mathbf{u}, \mathbf{A}_\Omega>, \tilde{U}^\Omega = <\mathbf{u}, \mathbf{A}^\Omega>$ .The $\tilde{U}^\Omega$ and $\tilde{U}_\Omega$ are *contravariant* and *covariant* surface components, also $\mathbf{A}^\Omega$ and $\mathbf{A}_\Omega$ are *contravariant* and *covariant* base vector, respectively. As it mentioned before in chapter 2, there is no difference between the *contravariant* and *covariant* coordinates of **u** with respect to $\mathbf{A}_3$ and $\mathbf{a}_3$, i.e. $\tilde{U}^3 = \tilde{U}_3 = <\mathbf{u}, \mathbf{N}>$. In such a case, the displacement vector can be decomposed into the tangential base vectors and the unit normal vector of the *reference* state $\mathbf{u} = \tilde{U}^\Omega \mathbf{A}_\Omega + \tilde{U}^3 \mathbf{A}_3 = \tilde{U}_\Omega \mathbf{A}^\Omega + \tilde{U}^3 \mathbf{A}_3$. In order to compute the *surface deformation tensor of first* kind it is necessary to know the continuous field of displacement vectors. The problem that we confronted with is of the following type: Typically, geodetic observations are usually discrete and consequently, the displacement vectors, deduced from the geodetic data, are of discrete nature. Assuming that a sufficient number of appropriately distributed discrete data is available, continuous information in space and time has to be estimate by computing best interpolation or approximation of the unknown functions over the given discretisation. The *finite element method* has been introduced as a powerful and widely used numerical technique dealing with this kind of problem. Accordingly, the modelling of surface component of displacement vector $\tilde{U}(\Lambda,\Phi)$ is approximated by a set of triangles. Figure 4-1 represents optimal *Delaunay* triangulation across the Southern *California* area, whose points of network are solutions of the *Scripps Orbit and Permanent Array Centre (SOPAC)*. For illustration of figures, the *Albers Conic map projection* has been chosen. It is a conic, equal-area projection, in which parallels are unequally spaced arcs of concentric circles. The parallels are more closely spaced toward north and south edges of the map. Meridians are equally spaced radii about a common center, and cut the parallels at right angles. The two standard parallels are free of angular and scale distortion. The distortion will be constant along any parallel and small for the area between two standard parallels. In each triangle, a characteristic form of the displacement field could be developing by a linear function of geodetic latitude and longitude approximates surface component of the displacement vector of type

$$\tilde{U}(\Lambda,\Phi)-\tilde{U}(\Lambda_0,\Phi_0)=A+B(\Lambda-\Lambda_0)+C(\Phi-\Phi_0) \qquad (4.2)$$

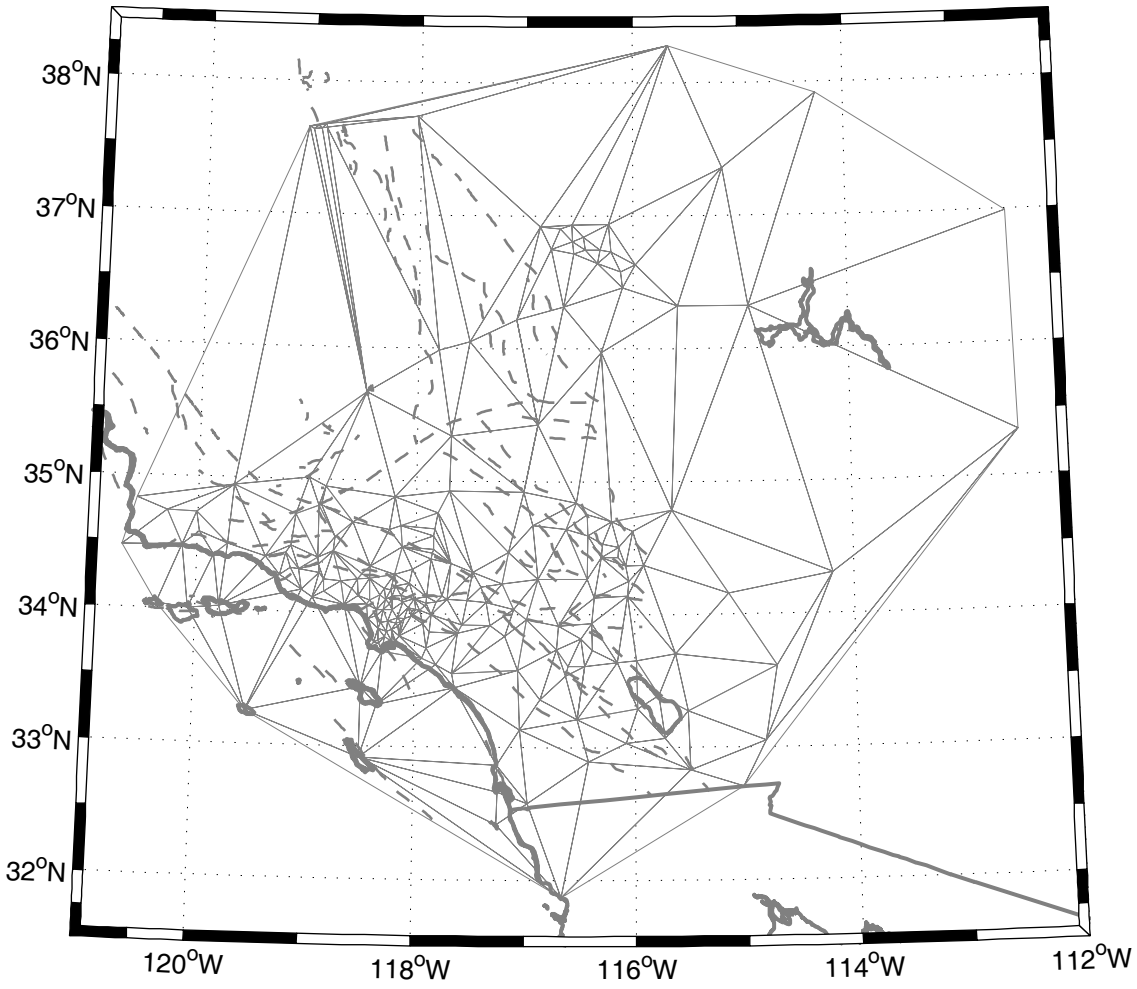


Fig.4-1: Triangulation across the Southern *California*. Figure is illustrated in *Albers Conic Equal-Area Projection* with center of projection at $116.5^0 W / 35^0 N$ with standard parallels $33^0 N$ and $37^0 N$ on reference ellipsoid $GRS80$.

Here $\tilde{U}(\Lambda,\Phi)$ is the surface component of the displacement vector in specific nodal points in an associated triangles and $\tilde{U}(\Lambda_0,\Phi_0)$ are the surface components of the displacement vector at the geometrical central point $P_0$ in the correspond element. Then, by means of equation (4.2) in every triangle, partial derivatives of the surface components of the displacement are obtainable. The next step is the computation of the height above the *reference ellipsoid* as a function of surface curvilinear coordinates, $\tilde{H}(\Lambda,\Phi)$ and its partial derivatives. It is done by using the height information through the *National Elevation Dataset (NED)* across the Southern *California*. The information can be freely download from the internet: (http://seamless.usgs.gov/website/seamless/). As a higher-resolution

product, we made use of *NED 1/3 Arc Second*, which has a resolution of approximately 10 meters. Vertical datum of this kind of data is *North American Vertical datum* of 1988 (*NAVD88*), on the other hand, our geodetic coordinates computed with respect to the *GRS80 reference ellipsoid*. Hence, we should convert *NAVD 88* to the height above the *GRS80 ellipsoid*. This is done by using of the latest geoid model *GEOID03* that is also available on the internet under: (http://www.ngs.noaa.gov/GEOID/GEOID03/). The *GEOID03* model is known as a *hybrid* geoid model, combining gravimetric information with GPS ellipsoidal heights on leveled benchmarks. The *GEOID03* model is developed in order to support the direct conversion between ellipsoidal heights and *NAVD 88* orthometric heights. For interpolating the height and deriving its partial derivatives with respect to the surface curvilinear coordinates in any computation point, we consider the element trial solution to be a linear 2-dimensional polynomial in our straight-sided triangular-shaped elements based on three *NED* points in the nearest neighborhoods of the computation point

$$\tilde{H}(\Lambda,\Phi)-\tilde{H}(\Lambda_0,\Phi_0)=A_1+A_2(\Lambda-\Lambda_0)+A_3(\Phi-\Phi_0) \qquad (4.3)$$

Here $\tilde{H}(\Lambda,\Phi)$ is the *height function* for the computation point and $\tilde{H}(\Lambda_0,\Phi_0)$ is the *height function* at the geometrical central point in the corresponding element. The coefficients $A_1, A_2, A_3$ are determined for each unknown function, based on the nodal values of the function. Here we compute the scalar functions of the elements of the surface deformation tensors, which are invariant referring to the change of surface coordinates. In other words, associated invariants should have evident physical interpretations. We should emphasize here that in contrast to the classical 2-dimensional planar deformation analyses, which components of the strain tensor have direct physical interpretations, we could not proceed in this way due to the curvilinear nature of the method of analysis. It is well known fact in matrix algebra which eigenvalues are invariant quantities independent of selected coordinate. Thus by applying the *general eigenvalue problem* of *surface strain tensor* [*Grafarend* 1995] and extract, the eigenvalues of *Euler-Lagrangian strain tensor* in the following way (denoted with primes)

Box 4-1 : *Eigenvalues of left versus right Euler-Lagrange deformation tensor of first type(principal stretches)*

*Left Eigenvalue of Euler-Lagrange Deformation Tensor*

$$\Lambda'_{1,2} = \frac{1}{2}\left\{ trace(E_{\Omega\Phi}\, A_{\Omega\Phi}{}^{-1}) \pm \sqrt{(trace(E_{\Omega\Phi}\, A_{\Omega\Phi}{}^{-1}))^2 - 4det(E_{\Omega\Phi}\, A_{\Omega\Phi}{}^{-1})} \right\} \quad (4.4)$$

*Right Eigenvalue of Euler-Lagrange Deformation Tensor*

$$\lambda'_{1,2} = \frac{1}{2}\left\{ trace(e_{\omega\phi}\, a_{\omega\phi}{}^{-1}) \pm \sqrt{(trace(e_{\omega\phi}\, a_{\omega\phi}{}^{-1}))^2 - 4det(e_{\omega\phi}\, a_{\omega\phi}{}^{-1})} \right\} \quad (4.5)$$

Contrary to the eigenvalues of the *Cauchy-Green deformation tensors* that are positive-definite property of deformation tensor, the eigenvalues of the *Euler-Lagrange deformation tensor* can be *negative* or *positive*. *Positive* principal strain refers to *extension* and *negative* principal strain refers to *compression*. Eigenvalues of *Euler-Lagrange strain tensor* represents the rates of *extensional* strain in principal directions; their sum defines the rate of *surface dilatation* as a surface invariant by

$$\Upsilon = \Lambda'_1 + \Lambda'_2 = tr(E_{\Omega\Phi}\, A_{\Omega\Phi}{}^{-1}) \qquad versus \qquad \gamma = \lambda'_1 + \lambda'_2 = tr(e_{\omega\phi}\, a_{\omega\phi}{}^{-1}) \quad (4.6)$$

The *surface dilatation* is the relative change of area. The *surface dilatation* of zero corresponds to no change of area, surface dilatation of *positive* values relates to *expansion* of the area and *negative* dilatations correspond to a *reduction of the area*. Second well-known invariant is the *surface maximum shear strain*

$$\begin{aligned} \Xi &= \Lambda'_1 - \Lambda'_2 \qquad versus \qquad \xi = \lambda'_1 - \lambda'_2 \\ &= \sqrt{(tr(E_{\Omega\Phi}\, A_{\Omega\Phi}{}^{-1}))^2 - 4\det(E_{\Omega\Phi}\, A_{\Omega\Phi}{}^{-1})} \qquad = \sqrt{(tr(e_{\omega\phi}\, a_{\omega\phi}{}^{-1}))^2 - 4\det(e_{\omega\phi}\, a_{\omega\phi}{}^{-1})} \end{aligned} \quad (4.7)$$

where $\Xi$ and $\xi$ is the *shear* across the direction of its maximum value that has an *always-positive* sign. *Rotation around the normal* to the surface could be interpreted as the third component of the rotation vector along the unit normal vector to the surface, $\Psi / \psi$ which is related to the rotation tensor by the following way [*Pietraszkiewicz* 1977]

$$\Psi = \frac{1}{2}\varepsilon^{\Omega\Phi} R_{\Omega\Phi} \qquad versus \qquad \psi = \frac{1}{2}\varepsilon^{\omega\phi} r_{\omega\phi} \quad (4.8)$$

where

$$\begin{aligned} R_{\Omega\Phi} &= \frac{1}{2}(\tilde{U}_{\Omega|\Phi} - \tilde{U}_{\Phi|\Omega}) & r_{\omega\phi} &= \frac{1}{2}(\tilde{u}_{\omega|\phi} - \tilde{u}_{\phi|\omega}) \\ \tilde{U}_{\Omega|\Phi} &= \tilde{U}_{\Omega,\Phi} - \Gamma^{\Theta}_{\Omega|\Phi}\tilde{U}_{\Theta} & \tilde{u}_{\omega|\phi} &= \tilde{u}_{\omega,\phi} - \Gamma^{\theta}_{\omega|\phi}\tilde{u}_{\theta} \end{aligned} \quad (4.9)$$

Then

$$R_{\Omega\Phi} = \frac{1}{2}(\tilde{U}_{\Omega,\Phi} - \tilde{U}_{\Phi,\Omega}) \qquad r_{\omega\phi} = \frac{1}{2}(\tilde{u}_{\omega,\phi} - \tilde{u}_{\phi,\omega}) \tag{4.10}$$

where $\varepsilon^{\Omega\Phi} / \varepsilon^{\omega\phi}$ are the contravariant components of *surface alternation tensor*, which are introduced in chapter 2 and $R_{\Omega\Phi} / r_{\omega\phi}$ are linearized *surface rotation tensors*. In analogy to the surface curvilinear coordinates of the displacement vector $\mathbf{u}$, it is possible to obtain surface curvilinear coordinates of the difference between the normal vectors in the *reference* surface and *current* surface $\mathbf{w}$. In the other word: $\tilde{W}_{\Omega} =< \mathbf{w} , \mathbf{A}_{\Omega} >, \tilde{W}^{\Omega} =< \mathbf{w} , \mathbf{A}^{\Omega} >$ .The $\tilde{W}^{\Omega}$ and $\tilde{W}_{\Omega}$ are *contravariant* and *covariant* surface components. As it mentioned before, there is no difference between the *contravariant* and *covariant* coordinates of $\mathbf{w}$ with respect to $\mathbf{A}_3$ and $\mathbf{a}_3$, i.e. $\tilde{W}^3 = \tilde{W}_3 =< \mathbf{w} , \mathbf{A}_3 >$. The vector $\mathbf{w}$ can be decomposed into the tangential base vectors and the unit normal vector of the *reference* state $\mathbf{w} = \tilde{W}^{\Omega}\mathbf{A}_{\Omega} + \tilde{W}^3\mathbf{A}_3 = \tilde{W}_{\Omega}\mathbf{A}^{\Omega} + \tilde{W}^3\mathbf{A}_3$. In order to compute the *surface deformation tensor of second kind* it is necessary also to know the continuous field of difference between the normal vectors in the *reference* surface and *current* surface. Moreover, the partial derivatives of a vector $\mathbf{w}$ can be derive as partial derivatives of surface components of the vector $\mathbf{w}$, by *finite element method* similar which illustrated in displacement vector $\mathbf{u}$. Comparing with the invariants of the *Euler-Lagrange deformation tensor of the first kind*, namely by considering the matrix representation of the curvature tensor to be symmetric, is more adequate to apply the general eigenvalue problem for obtaining the eigenvalues of *Euler-Lagrange deformation tensor of second kind* (denoted with double primes)

Box 4-2 : *Eigenvalues of left versus right Euler-Lagrange deformation tensor of second type*

*Left Eigenvalue of Euler-Lagrange Deformation Tensor*

$$\Lambda''_{1,2} = \frac{1}{2}\left\{ trace(K_{\Omega\Phi}\, A_{\Omega\Phi}{}^{-1}) \pm \sqrt{(trace(K_{\Omega\Phi}\, A_{\Omega\Phi}{}^{-1}))^2 - 4det(K_{\Omega\Phi}\, A_{\Omega\Phi}{}^{-1})} \right\} \tag{4.11}$$

*Right Eigenvalue of Euler-Lagrange Deformation Tensor*

$$\lambda''_{1,2} = \frac{1}{2}\left\{ trace(k_{\omega\phi}\, a_{\omega\phi}{}^{-1}) \pm \sqrt{(trace(k_{\omega\phi}\, a_{\omega\phi}{}^{-1}))^2 - 4det(k_{\omega\phi}\, a_{\omega\phi}{}^{-1})} \right\} \tag{4.12}$$

where $K_{\Omega\Phi} / k_{\omega\phi}$ is the *Euler-Lagrangian deformation tensor of second kind*. The correspondent eigenvalues are named *principal curvatures*. *Gaussian curvature* and *mean curvature* are two well-known invariants of deformation tensor of the second kind, which can be determined as two geometric invariants associated with the curvature tensors. *Gaussian curvature* is unaffected by the change of sign of the unit normal vector while the *mean curvature* reflects this change. This significant invariance property of the *Gaussian curvature* function, beside its invariant nature with respect to a change of surface coordinates, makes it the most appropriate tool to determine the geometry of the surface. Therefore, the differences of the *Gaussian* or *mean curvatures* of the *current*- and *reference* surface are considered more appropriate surface deformation measures, which can be obtained by the following way

$$h - H = \frac{1}{2}(a^{\omega\phi} b_{\omega\phi} - A^{\Omega\Phi} B_{\Omega\Phi}) \tag{4.13}$$

In this study we assumed geometry of reference surface is known and deformation of the surface are treated in *Lagrangian* portray. The change of the *mean curvature* between its value in *reference* surface and *current* surface is

$$k - K = \frac{1}{2}(\varepsilon_{\delta\sigma}\varepsilon_{\theta\psi} b_{\delta\theta} b_{\sigma\psi} - \varepsilon_{\Delta\Sigma}\varepsilon_{\Theta\Psi} B_{\Delta\Theta} B_{\Sigma\Psi}) \tag{4.14}$$

where k is the *mean curvature* in the *current* surface and K is the *mean curvature* in the *reference* surface.

# Chapter 5

## Surface Deformation Patterns of Southern California

The efficiency of proposed methods in last chapters in viewpoint of deterministic solutions in order to modelling of the surface deformation is demonstrated here by analysis of the real data set. The test area, namely southern California is the very famous region at the point of seismicity events. Another reason of choosing this region is that it include very dense networks of *GPS* stations with daily solutions in several years ,which is free available through the internet .Various surface deformation patterns are computed and compared with the results of seismicity map of this region .

## 5-1.Tectonic setting

Southern *California,* illustrated in figure 5-1, is a region of high seismicity and widely distributed active faulting. The relative plate motion between the *Pacific* and *North American* cause a highly complex system of sub-parallel transform faults to accommodate the right lateral motion of $50\,mm/yr$. Model of global plate motions range *from* 48 $mm/yr$ in terms of right lateral shear in *Central California,* namely parallel to the *Central San Andreas Fault* [*DeMets et al.,* 1987] *to* only 38 $mm/yr$ on or near *San Andreas Fault*. Another result of about 8 $mm/yr$ (15% of the relative plate motion) is documented by the 50-100 km wide Eastern *California* Shear Zone (*ECSZ*) which extends N35W from the eastern end of the *Big Bend* to the *Owens Valley* along a small circle about the *Pacific –North American pole of rotation* [*Savage* 1990]. The Southern part of the *ECSZ* is the site of *largest seismic* events, which in recent years has hit Southern *California* strongest. The large recent earthquakes occurred in the *ECSZ* of strength $M_W$ 7.3 (*Landers* 1992), and $M_W$ 7.1 (*Hector Mine* 1999). Both of them were right lateral strike-slip events in direction of NNW, trending subvertical faults, close in space and time, especially in a region where earthquakes recur every thousand years. The *Landers* and *Hector Mine* earthquakes have indeed provided important data on postearthquake deformation. Viscoelastic models have been proposed to explain the post-seismic relaxations following the *Landers* [*Pollitz et al.,* 2000] and *Hector Mine* [*Pollitz et al.,* 2001] earthquakes. However, any extrapolation of the available post-seismic earthquake data *does not suggest* that the velocities in the *Landers array* will return to their pre-*Landers* values soon [*Savage et al.,* 2003].

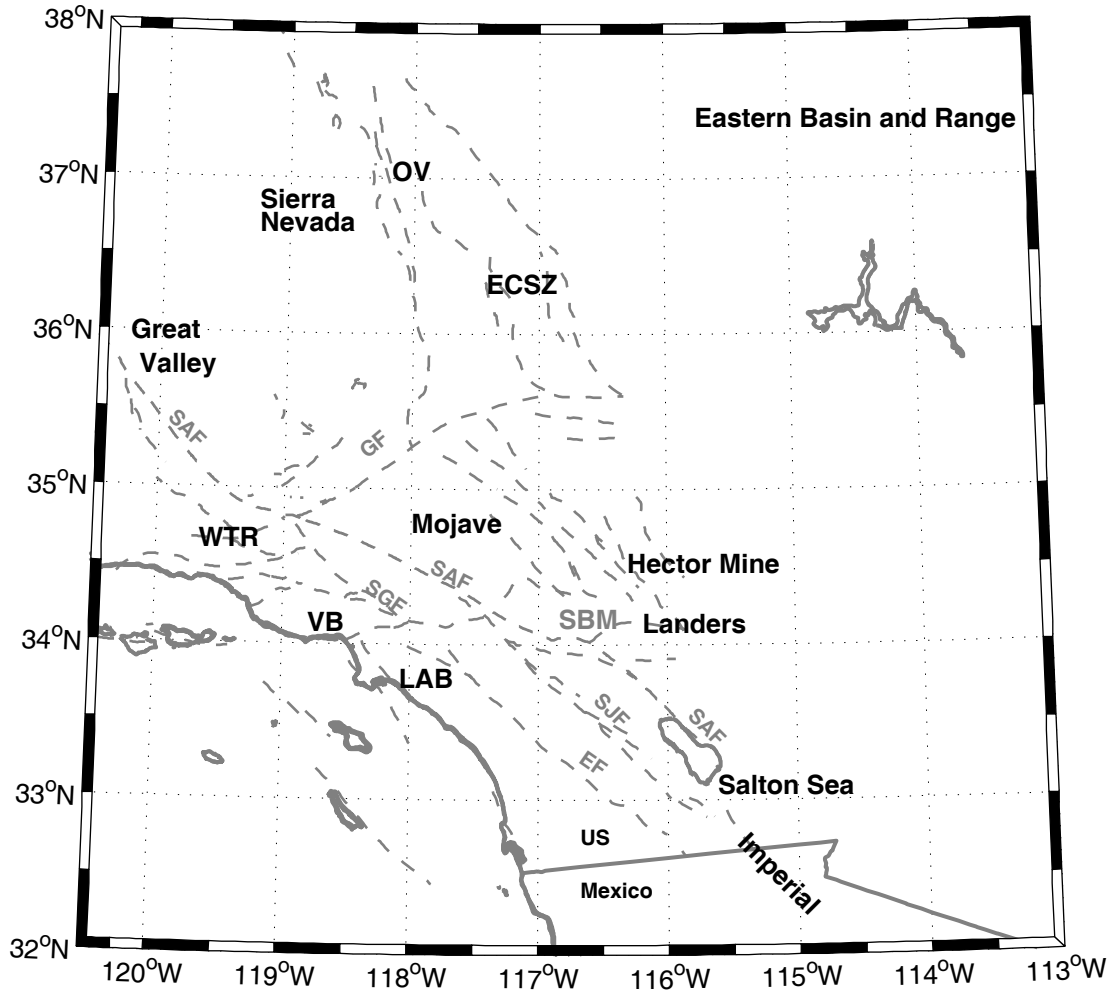


Fig.5-1: The Southern *California* Fault summarizes *San Andreas Fault (SAF), the Garlock fault (GF), the San Jacinto fault, the San Gabriel fault (SGF), the Elsinore fault (EF).* The mountain range extend from *San Bernardino* Mtns. Regions referenced in the text are the *Eastern California Shear Zone (ECSZ), the Owens Valley (OV), the Western Transverse Ranges (WTR), the Ventura Basin (VB), the Los Angeles Basin (LAB).* Figure is illustrated in *Albers Conic Equal-Area Projection* with center of projection at $116.5^0 W / 35^0 N$ with standard parallels $33^0 N$ and $37^0 N$ on reference ellipsoid $GRS80$.

On January 17th in 1994, *Northridge* $M_W$ 6.7 earthquake produced the largest ground motions in the *Los Angeles region.* The E-W striking sedimentary basin lies just south of the *Western Transverse Ranges,* a region influenced by the Big Bend in the north and characterized by E-W striking thrust faults, N-S shortening, and substantial uplift [*Namson et al.,* 1988]. Unlike the most strike-slip earthquakes along the Northwest trending faults in *ECSZ,* the *Northridge* earthquake was a deep thrust-type event with a strike of $122^0$ and a substantial up-dip component of slip [*Wald et al.,* 1996]. However, [*Stein et al.,* 1994] investigated possible stress triggering of the *Northridge* event by previous earthquakes. *Imperial Valley* extends from the southern end of the *San Andreas Fault (SAF)*

to the *United States – Mexico border*. It is one of the most seismically active portions of the *Pacific – North American plate* boundary. On October 15th in1979, a $M_W$ 6.9 earthquake occurred in this region. A relatively fast moving fault of estimated average slip rate along the Imperial Fault ranges from 15-20 $mm/yr$ based on shoreline deposits [*Thomas et al.,* 1996] to 35-43 $mm/yr$ based on conventional geodetic surveys [*Bennett et al.,* 1996; *Wdowinski et al.,* 2001] was documented. Geodetic investigations indicate that a rate of imperial Fault accommodates nearly 80% of the total plate motion between the *North American* and *Pacific Plates*. *InSAR* has also been used to land subsidence associated with geothermal fields in *Imperial Valley* [*Massonnet et al.,* 1997]. Figure 5-2 illustrates the seismicity map of the Southern *California* during the range of four years between January 2001 and January 2005, which can be getting through the *Southern California Earthquake Center (SCEC)* (http://www.scec.org). This figure shows earthquakes with magnitude bigger than three.

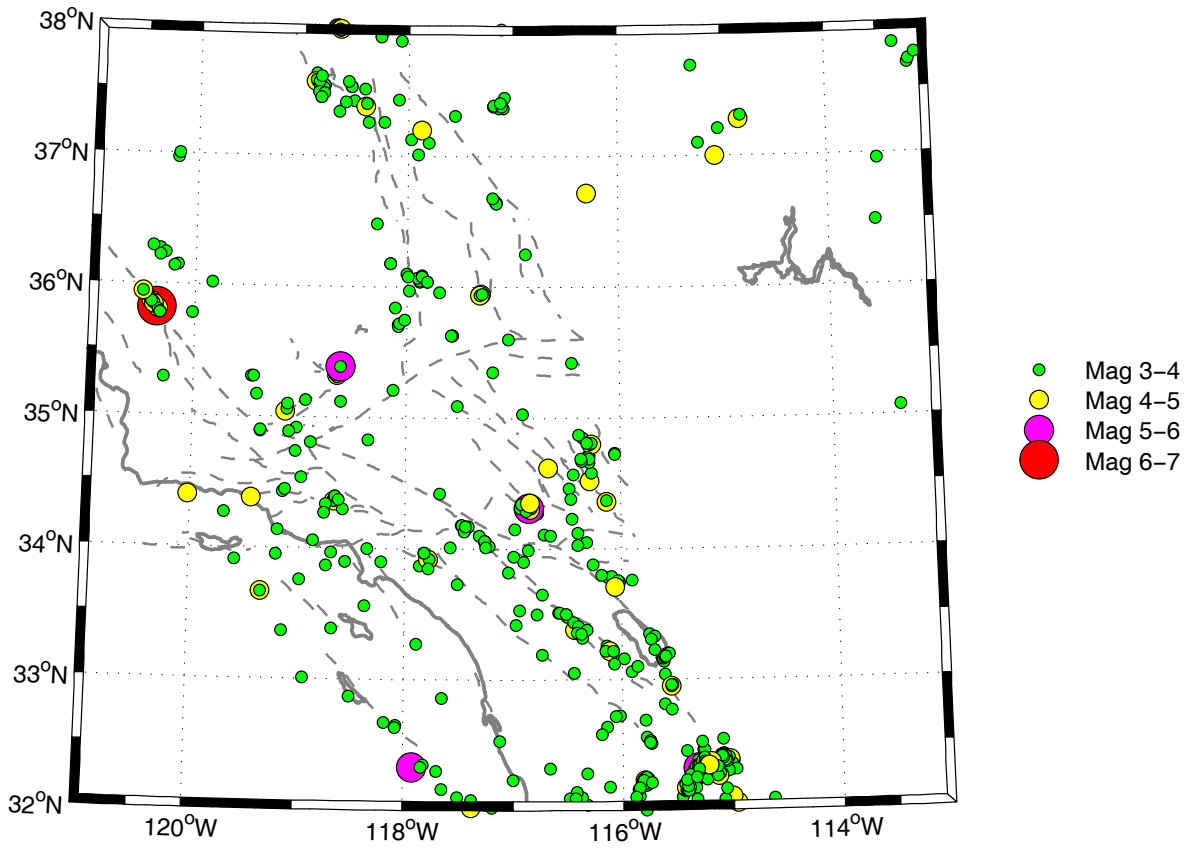


Fig. 5-2: Southern *California* seismic events with $M \geq 3$ from the *Southern California Earthquake Center* (January 2001 and January 2005) which are scaled by magnitude. Figure is illustrated in *Albers Conic Equal-Area Projection* with center of projection at $116.5^0 W / 35^0 N$ with standard parallels $33^0 N$ and $37^0 N$ on reference ellipsoid $GRS80$.

## 5-2. Data sets

Our GPS field observations are taken from *Scripps Orbit and Permanent Array Center (SOPAC)*, which include archive high-precision GPS data particularly for the monitoring of earthquake hazards tectonic plate motion, crustal deformation (http://sopac.ucsd.edu/).Given positions by *SOPAC* are provided in *ITRF2000* and *NAD83*, and include both horizontal and vertical velocities and their accuracies. All the chosen stations have individual and continuous solutions up to 4 years, between January 2001 and January 2005 and take into account the linear velocity between those epochs [*Nikolaidis* 2002]. Figure 5-3 illustrates the sites of *SOPAC* across the Southern *California*. We have chosen dense network of stations to get various surface deformation patterns of the Southern *California*.

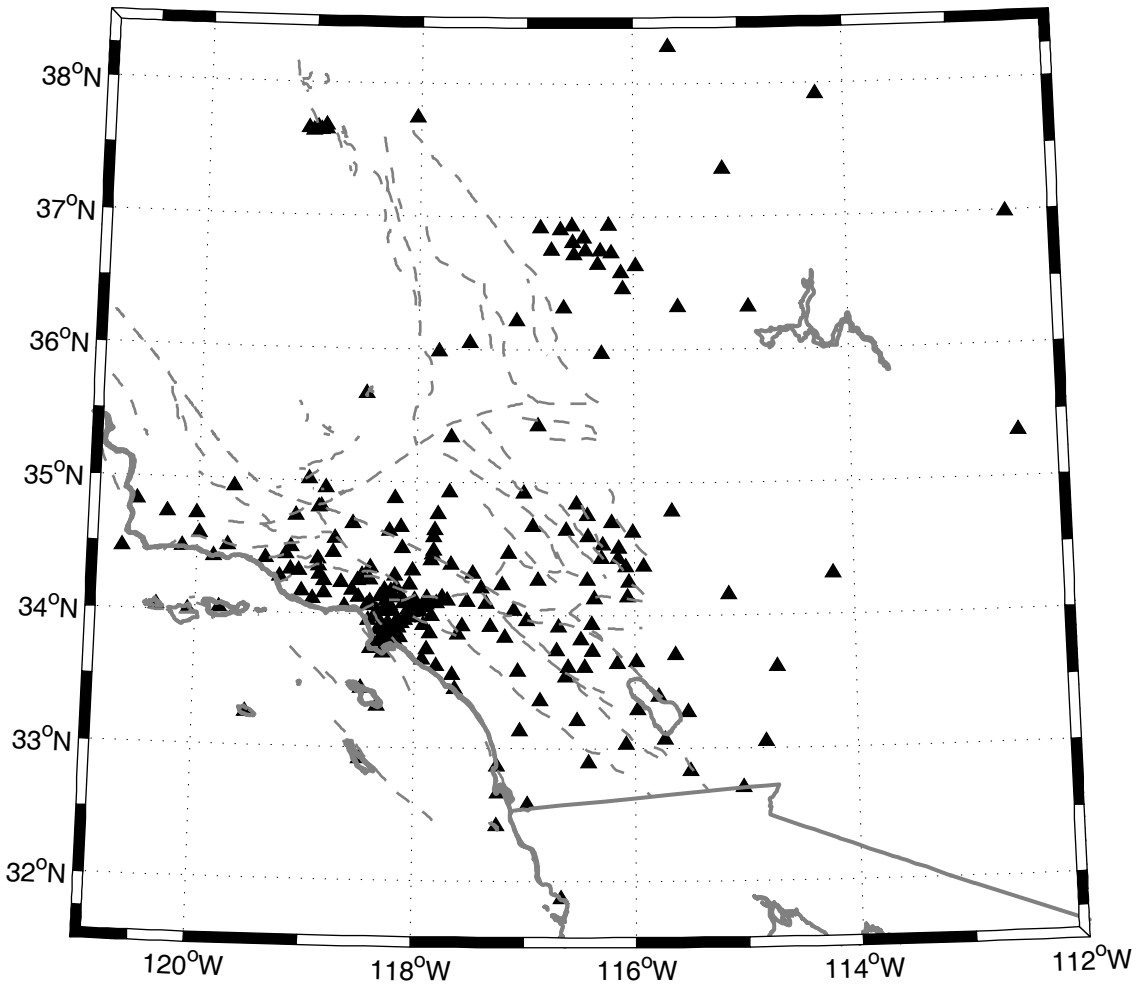


Fig.5-3: Sites of *SOPAC* network by individual solutions between 2001 and 2005. Figure is illustrated in *Albers Conic Equal-Area Projection* with center of projection at $116.5^0 W / 35^0 N$ with standard parallels $33^0 N$ and $37^0 N$ on reference ellipsoid $GRS80$.

Figure 5-4 illustrates horizontal velocity rates of the area assuming a stable *North America plate*. The velocity field reaches a value of approximately 48 $mm/yr$ in terms of *right lateral shear* in the central and western part of *California*, roughly parallel to the central *San Andreas Fault* [*DeMets et al.,* 1987].Well documented are the velocity fields in the *Coast Ranges*, namely larger than in the central parts. We have made an alternative, interpreting the Earth's discrete surface by adopting Figure 5-5, which illustrates the rates of vertical motion in Southern *California*. We have documented a *maximum magnitude of the subsidence* of the order ~ -10 $mm/yr$ for the *Los Angeles Basin* area. Another land subsidence has been observed in *Western Transverse Ranges*, rather across the *Coso Range* and the *North West of Salton Sea*, (namely) due to the geothermal activity in those regions. Notable *upward motions* can be seen in the *Landers* and *Hector Mine*, probably due to postseismic effects.

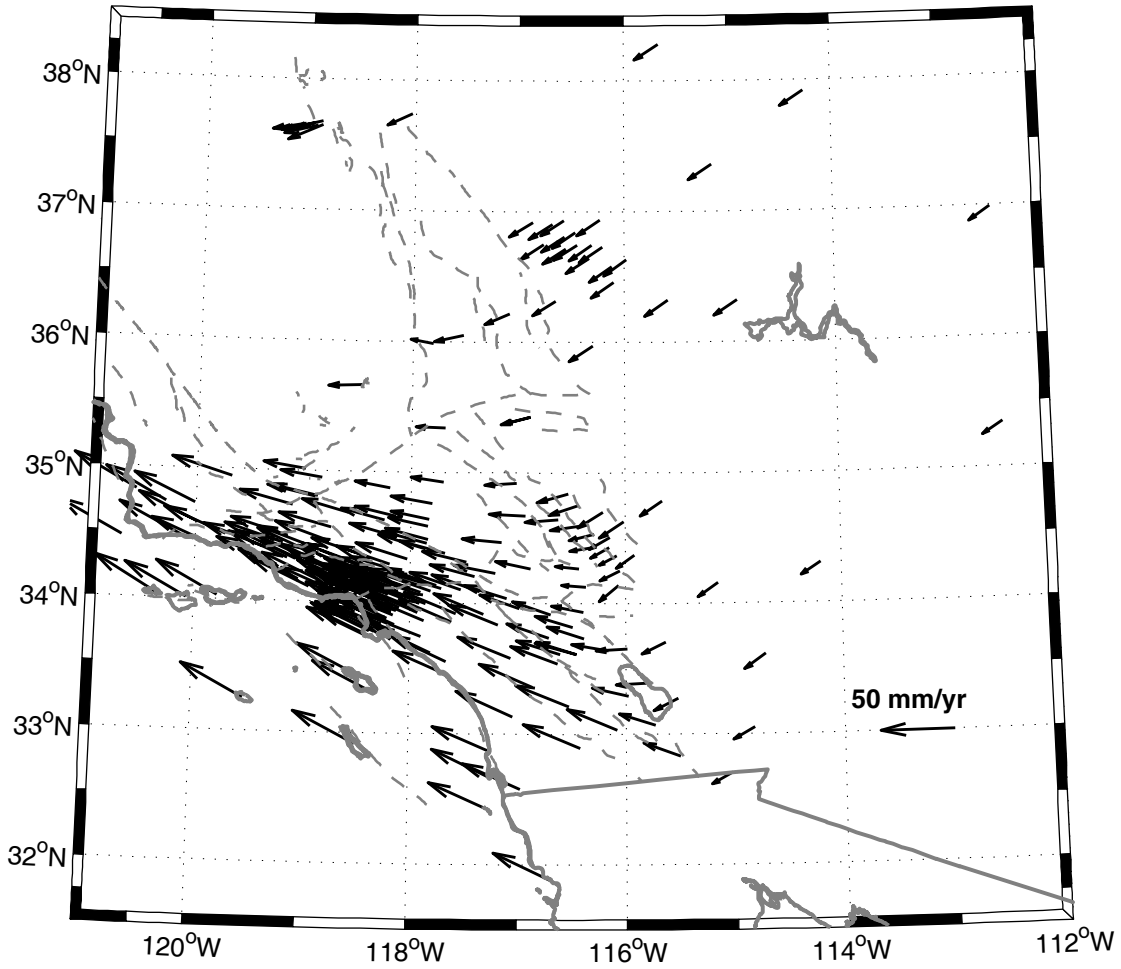


Fig.5-4: Horizontal rates of Southern *California* with respect to stable *North American plate* $mm/yr$. Figure is illustrated in *Albers Conic Equal-Area Projection* with center of projection at $116.5^0 W / 35^0 N$ with standard parallels $33^0 N$ and $37^0 N$ on reference ellipsoid $GRS80$.

Obviously, vertical components of motion cannot give us much information as other motion pictures.

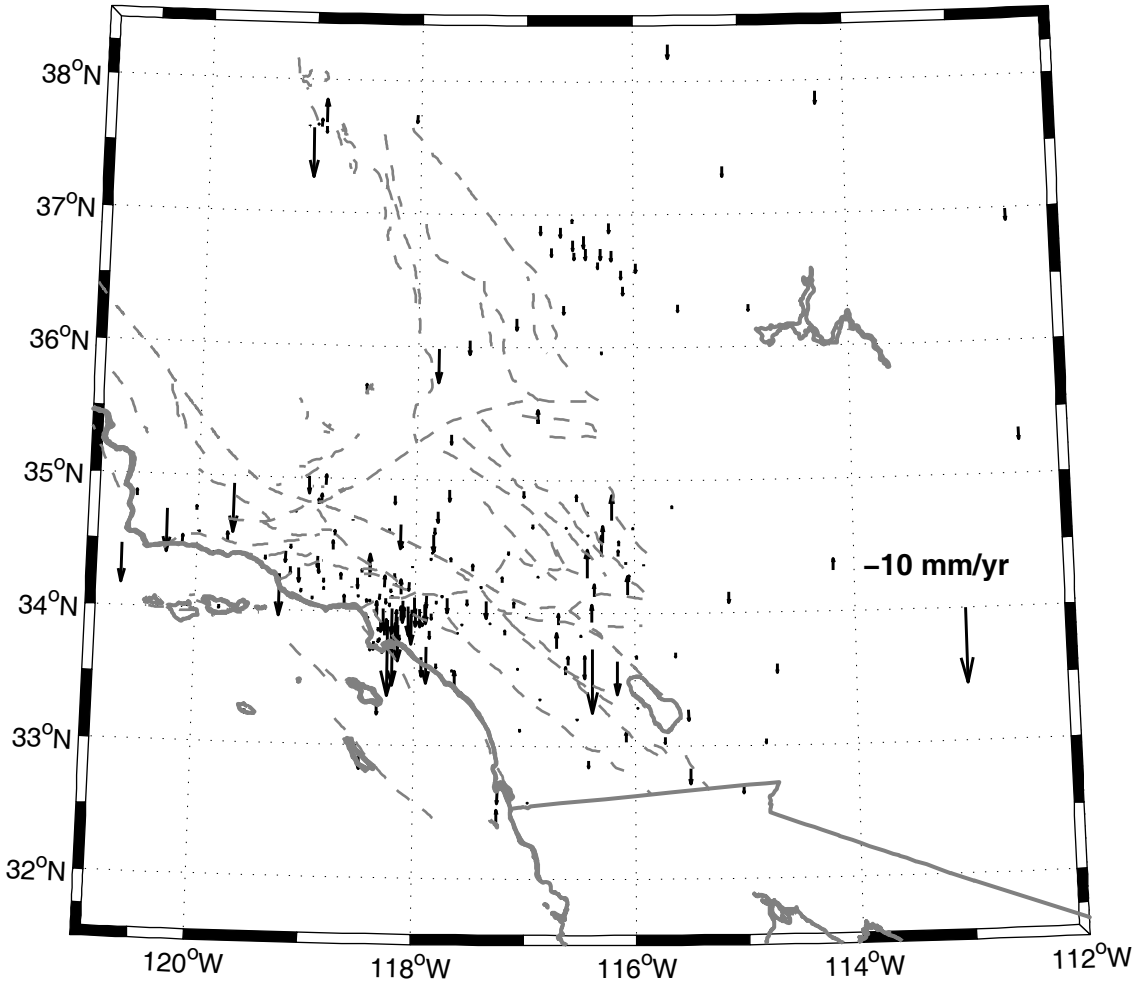


Fig.5-5: Rate of vertical motions in Southern *California* in $mm/yr$. Figure is illustrated in *Albers Conic Equal-Area Projection* with center of projection at $116.5^0 W / 35^0 N$ with standard parallels $33^0 N$ and $37^0 N$ on reference ellipsoid $GRS80$.

## 5-3. Analytical results

The numerical results are collected in the *Matlab* software package. We most emphasize that we think it of advantage to precisely contouring the key patterns in suitable map projections. Our results are represented in figures 5-6 to 5-15. In monitoring these patterns, we observe outliers, which are due to the weak geometry of underlying triangular elements. Figure 5-6 represents the *maximum geodetic surface strain rate* in the unit $10^{-7}/yr$, in detail across the Southern *California*. It represents the absolute magnitude of the largest eigenvalue in terms of *Euler-Lagrangian surface strain rate tensor*, given by (4.4):

$$\varepsilon_{\max}(\Phi,\Lambda) = \max[abs(\Lambda_1'(\Phi,\Lambda)), abs(\Lambda_2'(\Phi,\Lambda))] \qquad (5.1)$$

Namely, following [*Ward* 1998a, 1998b], it represents the total deformation measure, also in cases where only horizontal motions are available. In the following figures, traces of the major quaternary faults are shown. The strongest *maximum of geodetic strain rates* is related to *Landers* area with the rate $4.7 \times 10^{-7} / yr$, the *Southern part of SGF* with rate $4 \times 10^{-7} / yr$, *Salton Sea* and *Imperial Valley* with rate $3.8 \times 10^{-7} / yr$. For most of the peaks are appearing near the *SAF*, however, it is revealing that the entire *Los Angeles* and east-central *Ventura Basin* also exhibits a high *maximum geodetic strain rate* of the order $4.2 \times 10^{-7} / yr$.

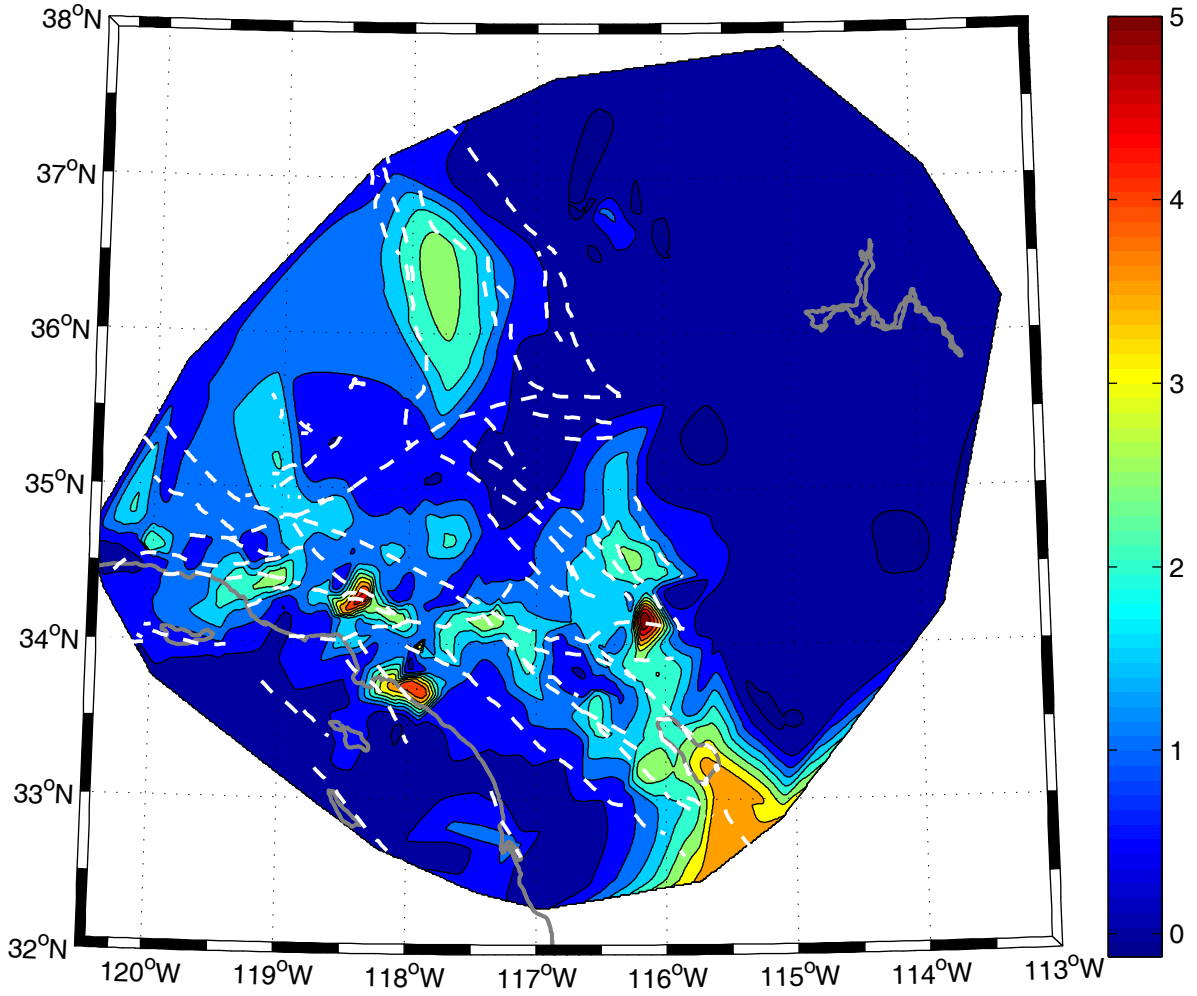


Fig.5-6: *Maximum geodetic surface strain rate* in the Southern *California* in unit $10^{-7} / yr$ .Faults are represented by white dashed lines and coastlines are represented by bold solid lines. Figure is illustrated in *Albers Conic Equal-Area Projection* with center of projection at $116.75^0 W / 35^0 N$ with standard parallels $33^0 N$ and $37^0 N$ on reference ellipsoid *GRS*80.

The pattern of *surface maximum shear strain rate* in units of $10^{-7}/yr$ is illustrated in figure 5-7. The *surface maximum shear strain* represents the *anisotropic* part of deformation tensor, which is clear from equation (4.7), and is considered a key deformation measure in understanding physical processes of the Earth's surface. The rate of *surface maximum shear strain* depicts a general similarity to correspondent *maximum geodetic strain rates*. The *surface maximum shear strain rates* have greater values than the *maximum geodetic strain rates*, which can be expected due to their mathematical formulations. The highest *surface maximum shear strain rate* lies in the area containing the creeping segments of *SAF*, the area containing *Salton Sea* with rate $6\times10^{-7}/yr$. High *surface maximum shear strain rates* are also observed at *the Southern San Gabriel fault, Hectore Mine, Landers, Los Angeles Basin* and *Ventura Basin, Owens Valley*. The regions of highest *surface maximum shear strain rate* are not on the major faults as would be expected, but rather in the regions surrounding previous earthquakes. Earthquakes in 1999 (*Hectore Mine, M 7.1*), 1994(*Northridge, M 6.7*), 1992 (*Landers,* M *7.3*), 1992(*Big Bear, M 6.4*), 1979 (*Imperial Valley,* M *6.4*), 1971(*San Fernando, M 6.6*), 1952 *(Kern County,* M *7.7*), 1942 (*Salton Sea aftershock, M 6.4*), 1933(*Los Angeles Basin, M 6.4*) and 1872 (*Owens Valley, M 7.6*) have apparently caused the largest strain reactions. The monitoring of this pattern at regions with high seismic activity, or regions that had experience of big earthquakes confirms the key role of the *surface maximum shear strain rate* in earthquake studies as well as the validity of the *surface maximum shear strain rate* pattern which is obtained based on the intrinsic Earth's surface deformation analysis. Figure 5-8 illustrates the pattern of *surface dilation rate*, in unit $10^{-7}/yr$. The sign of signals change depend on the elements of the surface area are in a state of *compression (negative values)* or *expansion (positive values)*. *Surface dilation* represents the *isotropic* part of deformation tensor. In the *surface dilatation* field, notable areas of compression are documented for *Los Angeles* about $-3.2\times10^{-7}/yr$ and for *Ventura Basin* about $-4.2\times10^{-7}/yr$. This contraction extends into the *Santa Barbara channel*, where its rate is $-2\times10^{-7}/yr$. Another pattern of compression appears in the *Southern Owens Valley* with rate $-2\times10^{-7}/yr$. Negligible compression can be seen in the southern part of *SAF Indio* with rate $-1\times10^{-7}/yr$, possibly associated with after effects of the 1940 *Imperial Valley* earthquake. Two strongest *positive*

*dilatational* signals appear to be associated the *Landers* with rate $4.3\times10^{-7}$ / *yr*; another is distributed between *the Southern Elsinore*, *San Jacinto faults* and *northern Imperial Valley fault* with rate $3.5\ \times10^{-7}$ / *yr*.

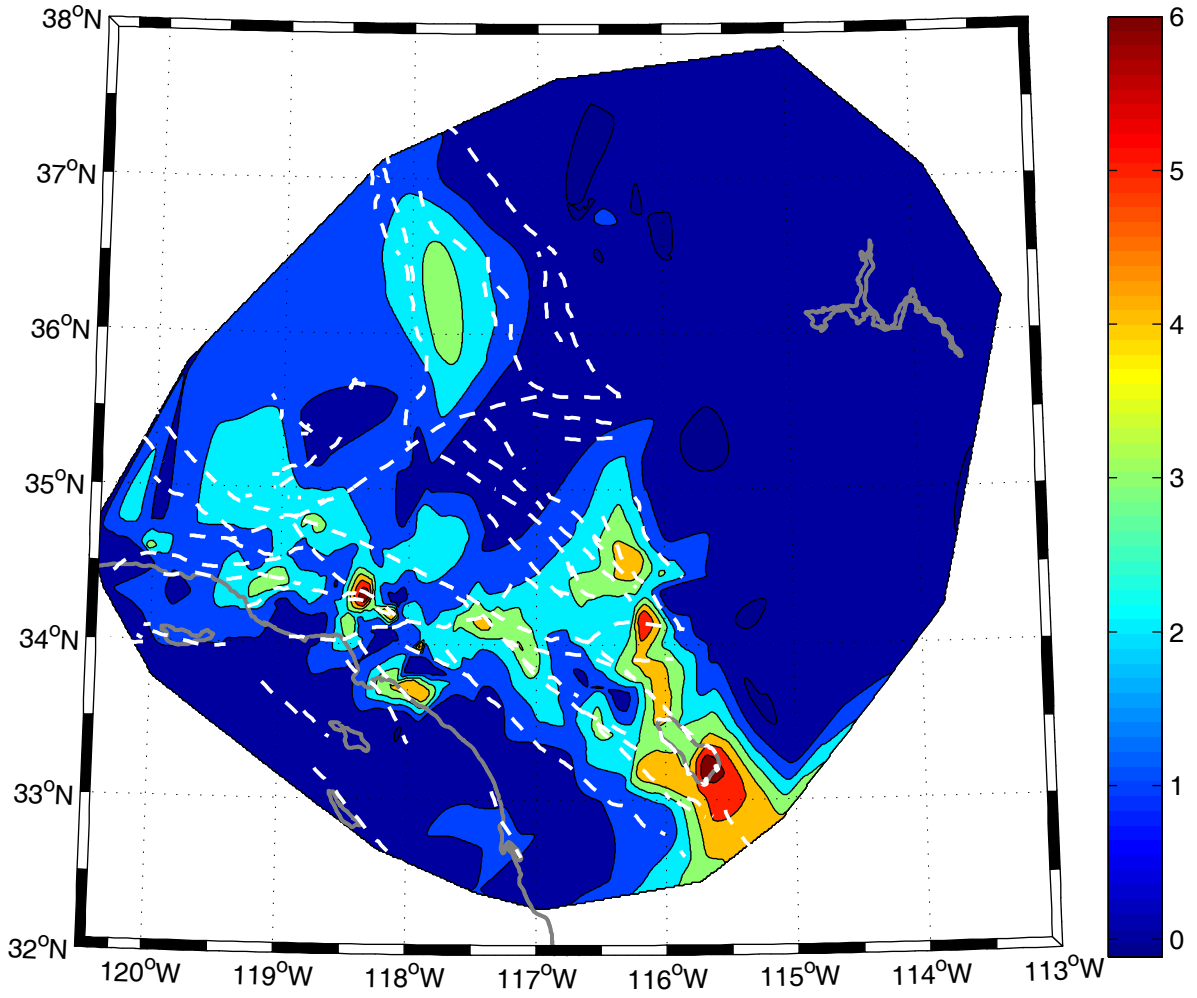


Fig.5-7:*Surface maximum shear strain rate* in the Southern *California* in unit $10^{-7}$ / *yr*. Faults are represented by white dashed lines and coastlines are represented by bold solid lines. Figure is illustrated in *Albers Conic Equal-Area Projection* with center of projection at $116.75^{0}W / 35^{0}N$ with standard parallels $33^{0}N$ and $37^{0}N$ on reference ellipsoid *GRS*80.

Another surface extension is documented across the *Southern San Gabriel Fault* with the rate $2\times10^{-7}$ / *yr*. The pattern of *surface dilatation* rates in the Southern *California* is generally consisting with previous studies that used geodetic data [e.g., *Johnson et al.*, 1994; *Snay et al.*, 1996; *Shen et al.*, 1997; *Shen- tu et al.*, 1999]. Many local peaks (or valleys) in the *dilatation rate* field occur in vicinities of recent earthquakes, which implies that much of the rapid spatial variation in

strain rate field is probably caused by transient deformation associated with recent earthquakes [*Shen et al.*, 1996]. The pattern of *the rates of the rotation around the normal* in unit $10^{-7}\ rad/yr$ is illustrated in figure 5-9.The *positive* values of rates are referred to *clockwise* rotation around the normal to the surface and the *negative* values are referred to *counter clockwise* rotation.

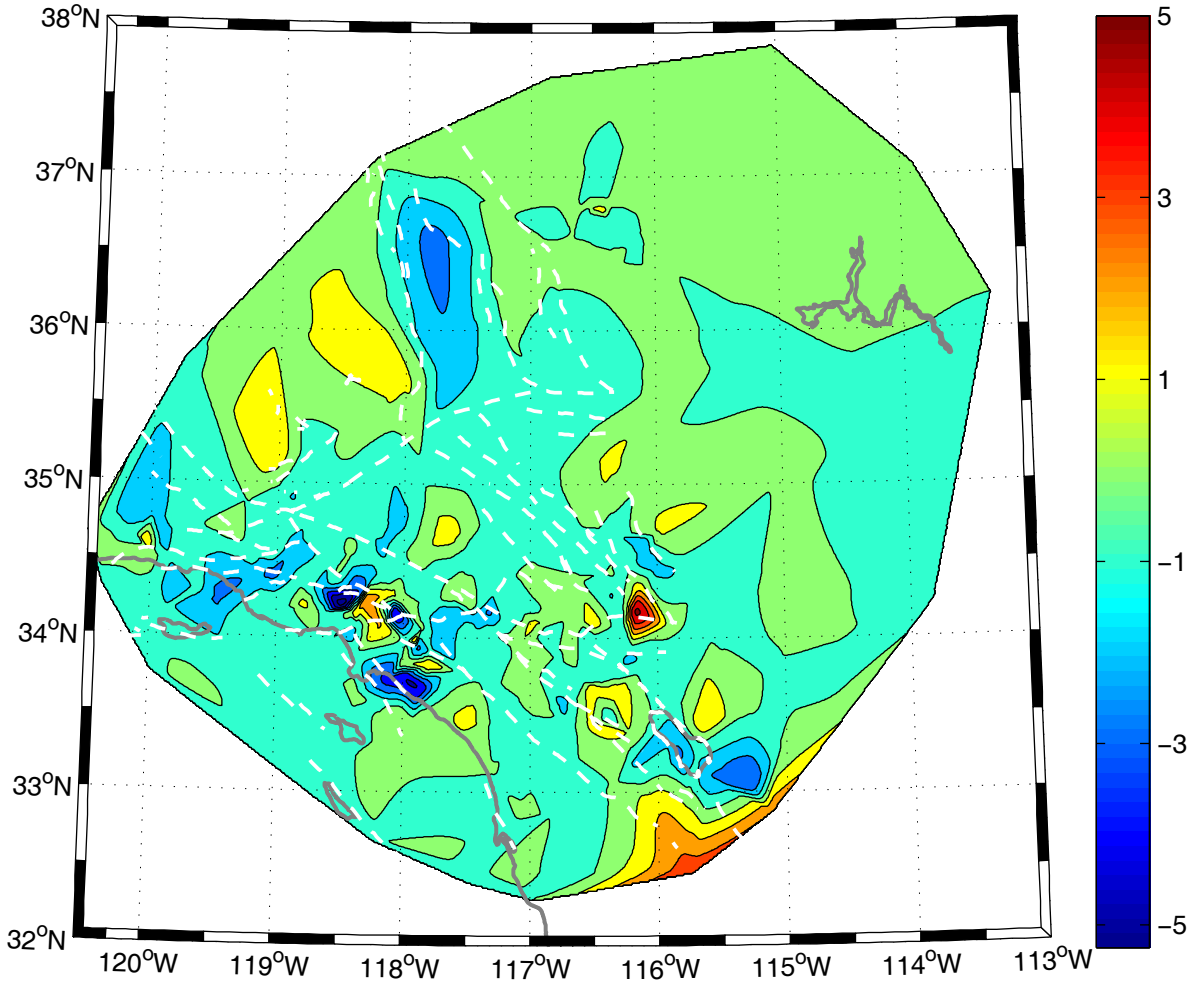


Fig.5-8: Surface dilation rate in the Southern *California* in unit $10^{-7}/yr$. Faults are represented by white dashed lines and coastlines are represented by bold solid lines. Figure is illustrated in *Albers Conic Equal-Area Projection* with center of projection at $116.75^0W/35^0N$ with standard parallels $33^0N$ and $37^0N$ on reference ellipsoid $GRS80$.

The pattern can detect signals of current kinematics of the area. Large rotation rates are found along the *SAF* and the *SJF*, as expected from active wrenching dislocations along the two faults. The highest *positive* rotation signals are detected over the *Landers* with the rate $2.7\times10^{-7}\ rad/yr$ and *Imperial Valley* with the rate $2.3\times10^{-7}\ rad/yr$. The highest rotation rates in the *Landers* and

*Imperial Valley* rupture areas are consistent with postseismic motions with the same sense as the main rupture. In the *Ventura Basin* region, it is monitored that the *clockwise* rotation are in the range between $0.1-1.5\times10^{-7}\ rad/yr$. Other studies support this idea e.g., [*Donnellan et al*, 1993]. The *eastern segment of Garlock fault* rotates *clockwise* at a rate of nearly $1.5\times10^{-7}\ rad/yr$. A very limited area in *Sierra-Nevada* shows a negligible *counter clockwise* rotation with the rate $0.1\times10^{-7}\ rad/yr$. Rather in the remote eastern part of *Mojave Desert* and the Southern *Mojave* region, *counter clockwise* rotation is documented with the rate $-0.5\times10^{-7}\ rad/yr$.

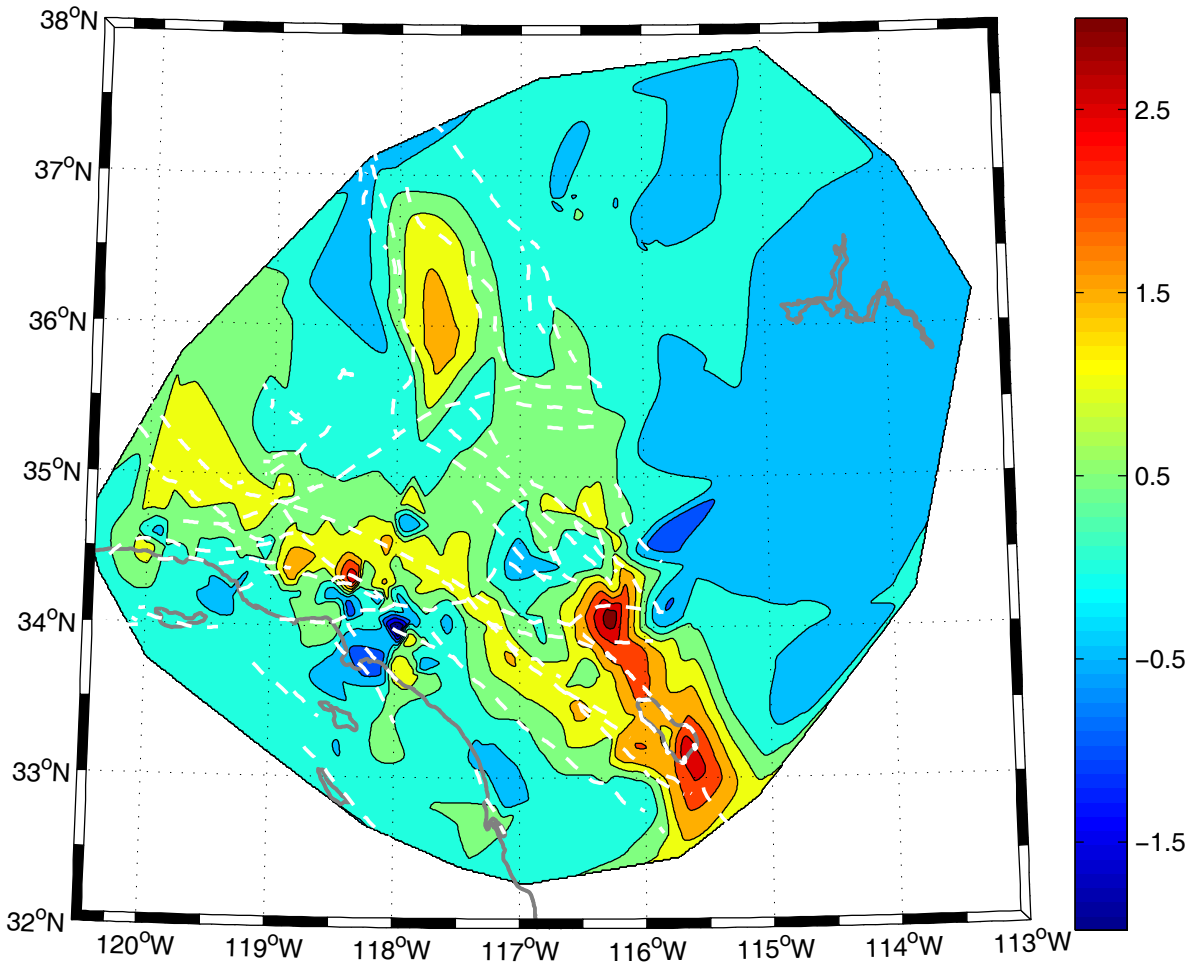


Fig.5-9: Rotation around the normal over the Southern *California* in unit $10^{-7}\ rad/yr$. Faults are represented by white dashed lines and coastlines are represented by bold solid lines. Figure is illustrated in *Albers Conic Equal-Area Projection* with center of projection at $116.75^{0}W/35^{0}N$ with standard parallels $33^{0}N$ and $37^{0}N$ on reference ellipsoid *GRS*80.

Figure 5-10 illustrates rates of *absolute rotation around the normal*. Comparison between figure 5-10 and the seismicity map of the area proves that the rotation around the normal as a deformation tool can

play a desirable role in earthquake investigations. The pattern of *difference of eigenvalues for Lagrangian tensor of second kind* $\Lambda''_{\max} - \Lambda''_{\min}$ over the Southern *California* is illustrated by figure 5-11. Referring to its definition, the difference is almost *positive* like the *surface maximum shear strain rates*. In general, this pattern is similar to the pattern of *surface maximum shear strain rates* and can detect areas with high surface deformations. The highest rates are monitored along *ECSZ in Landers and Hector Mine* with rates of nearly $0.011\ /m\ \ yr$ .

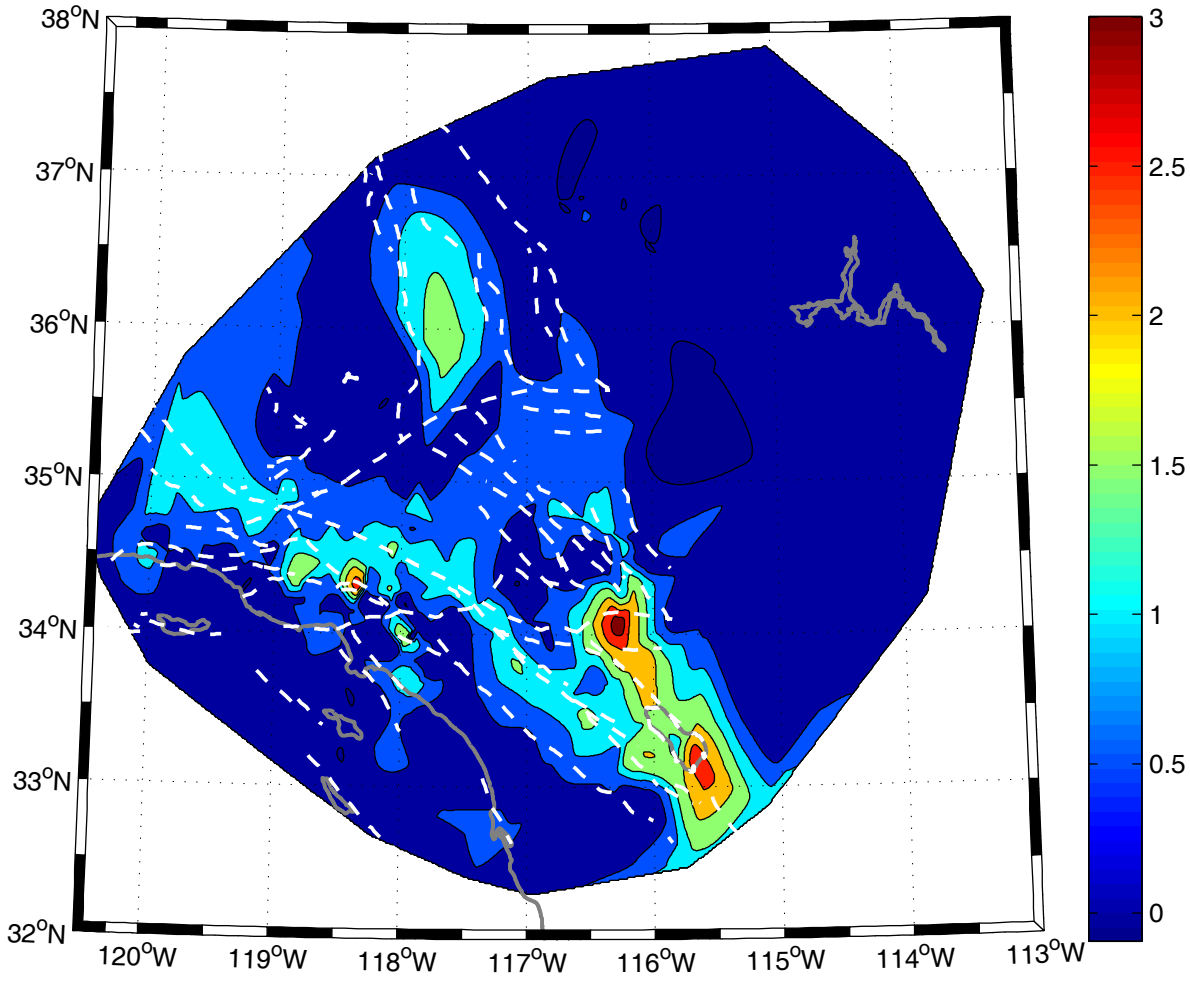


Fig.5-10: Absolute rotation around the normal in the Southern *California* in unit $10^{-7}\ rad\ /\ yr$ . Faults are represented by white dashed lines and coastlines are represented by bold solid lines. Figure is illustrated in *Albers Conic Equal-Area Projection* with center of projection at $116.75^{0}W\ /\ 35^{0}N$ with standard parallels $33^{0}N$ and $37^{0}N$ on reference ellipsoid $GRS80$ .

The *Salton Sea* area and *Imperial Valley* areas are covered by peaks with the rate $0.01\ \times 10^{-7}\ /m\ \ yr$ . Other patterns of high peaks detected referring to *Los Angeles* areas, *eastern of San Gabriel fault* and

*Owens Valley*. The very interesting feature of the pattern is a peak of values around southeastern part of *Basin and Range*, which it is not so detectable by the *surface maximum shear strain* rates while it is uncovered by the pattern of difference of eigenvalues *for Lagrangian tensor of the second kind*.

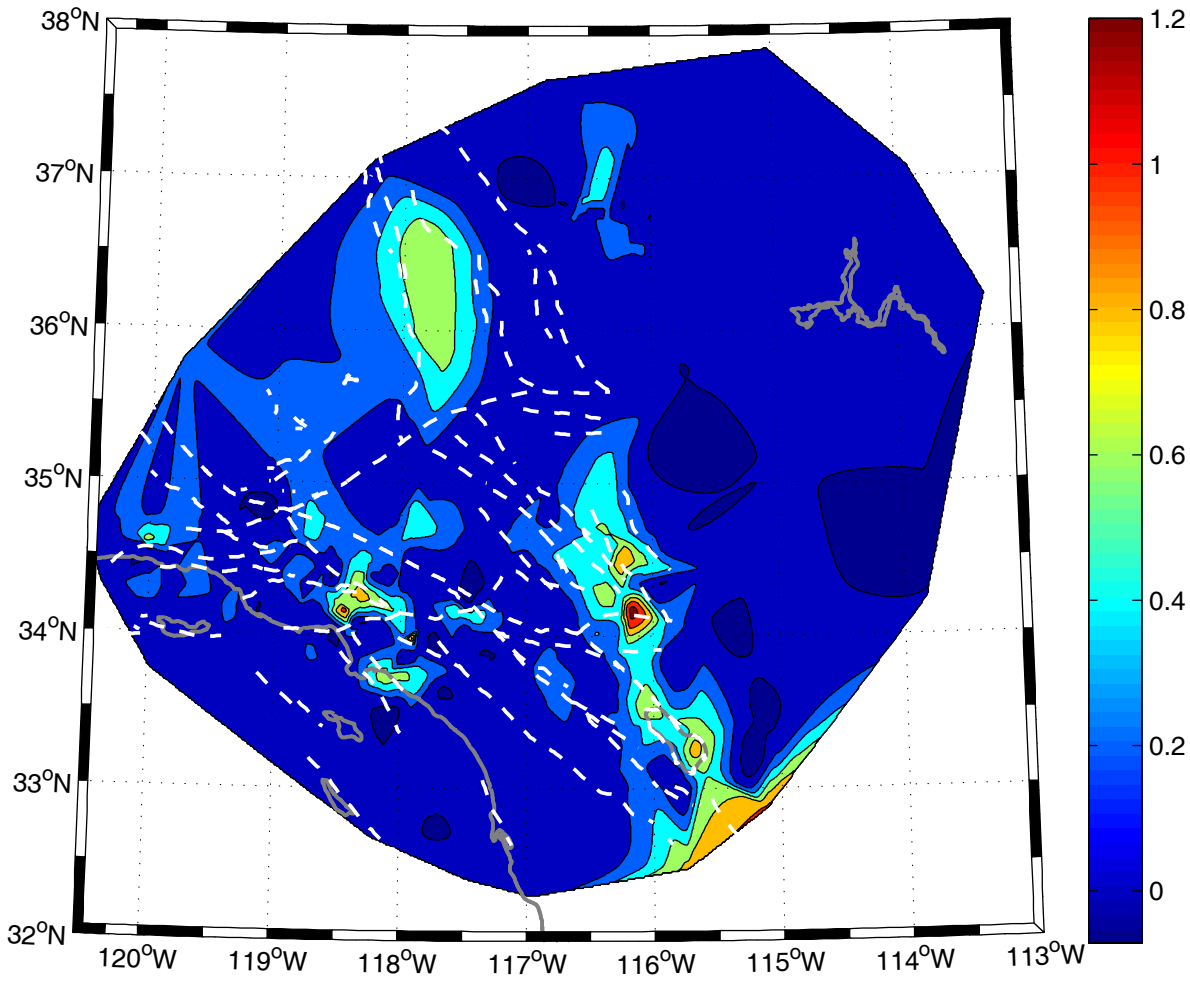


Fig.5-11: Difference of eigenvalues for *Lagrangian tensor of second kind* in the Southern *California* in unit $10^{-7}/m\ yr$ . Faults are represented by white dashed lines and coastlines are represented by bold solid lines. Figure is illustrated in *Albers Conic Equal-Area Projection* with center of projection at $116.75^0 W / 35^0 N$ with standard parallels $33^0 N$ and $37^0 N$ on reference ellipsoid $GRS80$.

In a different manner from difference of eigenvalues *for Lagrangian tensor of second kind*, the *sum of eigenvalues for Lagrangian tensor* $\Lambda''_{\max} + \Lambda''_{\min}$ can be *positive* or *negative*, which shown in figure 5-12. As mentioned in equation (4-13) and (4-14), we attached to our study, *Gaussian curvature* differences and *mean curvature* differences as scalar invariants of *second fundamental form of Lagrangian tensor*. *Positive* and *negative* values of these invariants are related to upward and downward motion of surface of the Earth. Figure 5-13 monitors the pattern of *difference of mean*

*curvature rates* before the deformation of the surface of the Earth and after the deformation in the unit $10^{-7} / m\ yr$. In this figure, *positive* values are connected to rising regions whereas *negative* values are related to sinking regions.

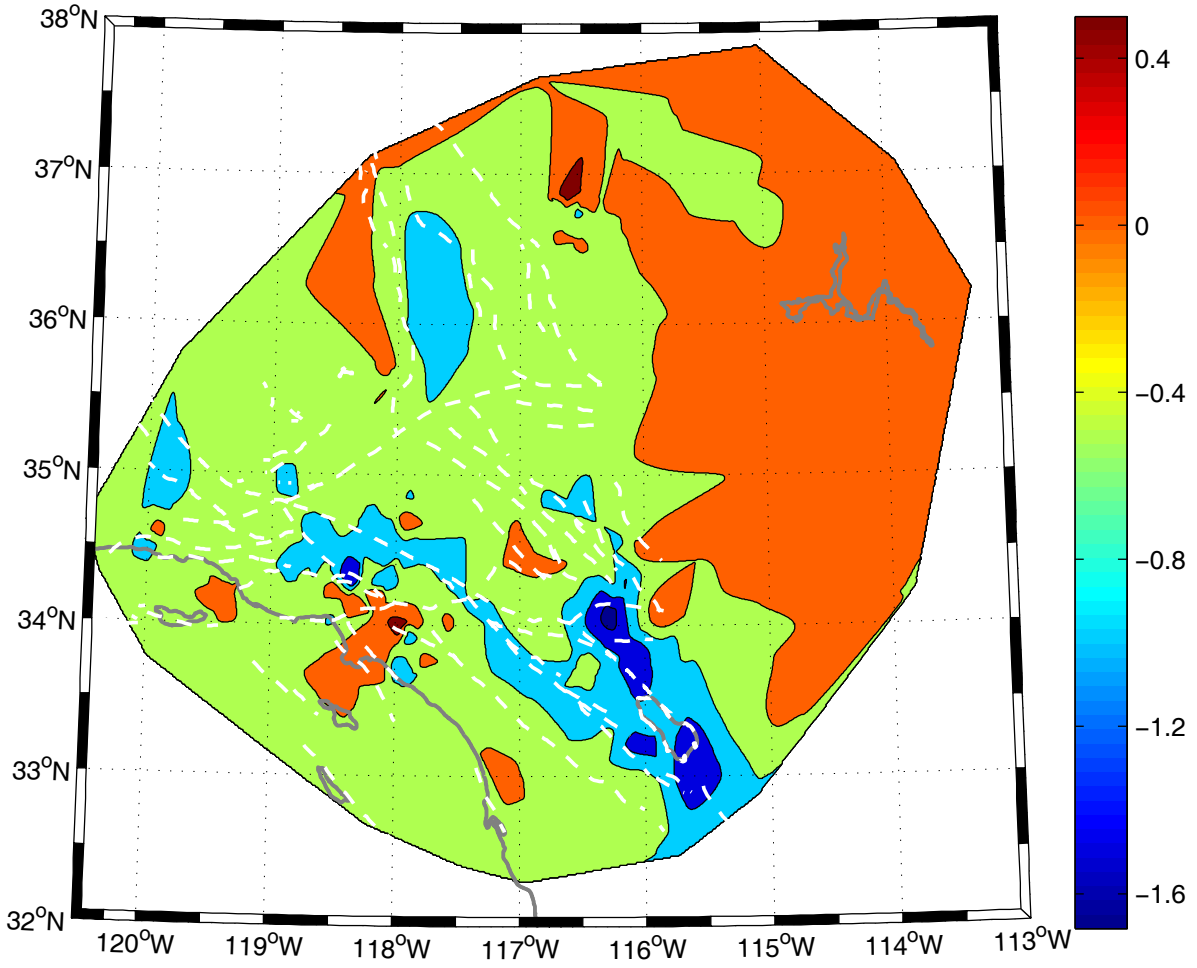


Fig.5-12: Sum of eigenvalues for *Lagrangian tensor of second kind* in the Southern *California* in unit $10^{-7} / m\ yr$. Faults are represented by white dashed lines and coastlines are represented by bold solid lines. Figure is illustrated in *Albers Conic Equal-Area Projection* with center of projection at $116.75^0 W / 35^0 N$ with standard parallels $33^0 N$ and $37^0 N$ on reference ellipsoid $GRS80$.

Regions undergoing to subsidence include the southern part of *Owens Valley*, the *southwestern part of Sierra-Nevada* and the *southeastern part of the Great Valley* and the *Los Angeles area*. Notable rising areas include *ECSZ* and the northeastern *part of Mojave Desert*. Figure 5-14 represents the pattern of *Gaussian curvature differences rates* in the unit $10^{-9} / m^2\ yr$. A comparison of figure 5-13 and figure 5-14 shows that the patterns of both maps are similar.

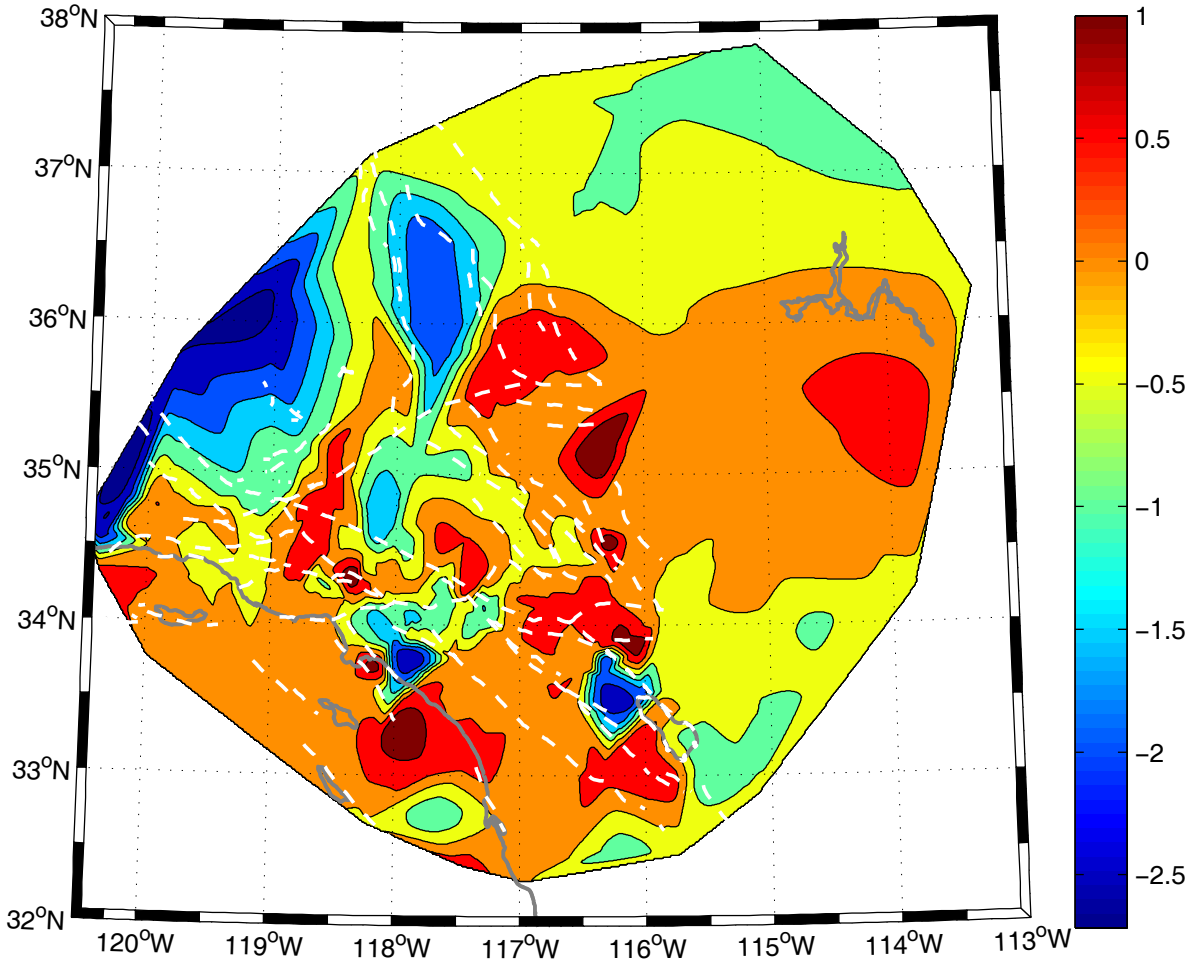


Fig.5-13: Difference of *mean curvature* in the Southern *California* in the unit $10^{-7}/m\ yr$. Faults are represented by white dashed lines and coastlines are represented by bold solid lines. Figure is illustrated in *Albers Conic Equal-Area Projection* with center of projection at $116.75^{0}W / 35^{0}N$ with standard parallels $33^{0}N$ and $37^{0}N$ on reference ellipsoid $GRS80$.

Figure 5-15 illustrates the *pattern of vertical components of the displacement* rates across the Southern *California* in the units of mm/yr obtained from differences of geodetic heights of centers of triangle elements in the finite element approach. *Positive* values are connected to upward motion of the surface of the Earth whereas *negative* values are related to downward motion of the surface of the Earth. The significant signals of sinking areas are apparent in the north - western part of the *Salton Sea* and the *Los Angeles Basin* with a rate of nearly $-2.4\,mm/yr$ and the southern part of *Owens Valley* with rate $-1.5\,mm/yr$.

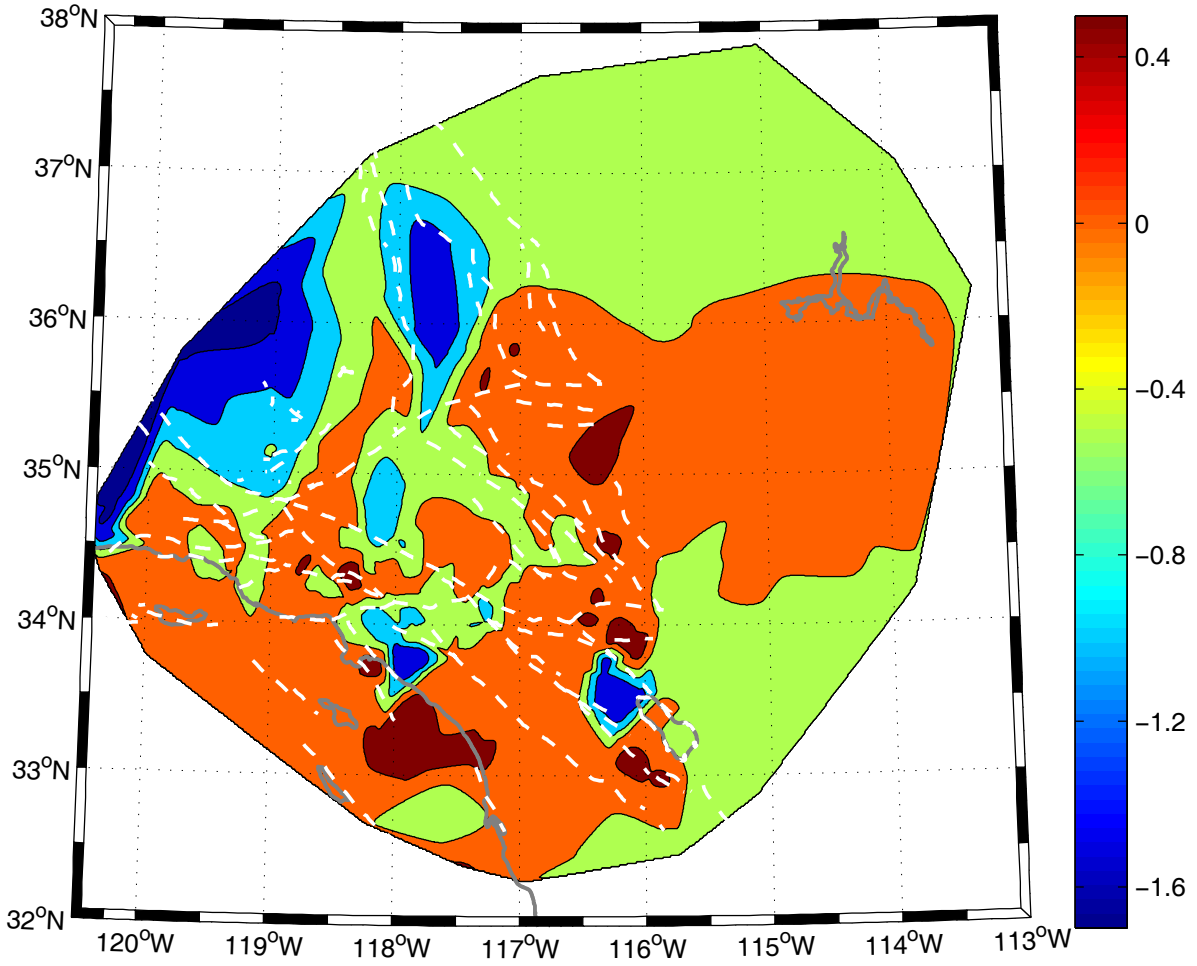


Fig.5-14: Difference of *Gaussian curvature* in the Southern *California* in the unit $10^{-9}/m^2\ yr$. Faults are represented by white dashed lines and coastlines are represented by bold solid lines. Figure is **i**llustrated in *Albers Conic Equal-Area Projection* with center of projection at $116.75^0 W / 35^0 N$ with standard parallels $33^0 N$ and $37^0 N$ on reference ellipsoid $GRS80$.

The strongest rising peaks appear in the *ECSZ* and north part of *Mojave Desert* with nearly $1 mm / yr$. Comparison of the patterns of vertical components of the displacement rates in figure 5-13, figure 5-14 and figure 5-15 indicates the ability of the pattern of *Gaussian curvature differences* and *mean curvature differences* to describe the motion of the surface of the Earth in *vertical* direction. In other words, spatial patterns of *Gaussian curvature differences* and *mean curvature differences* present a more reliable and accurate portray of the existing sinking and rising regions of the study area. It is can be considered as a powerful tool of the *Lagrange deformation tensor of the second kind* and its associated invariants in comparison to what can be extracted in this context from the vertical components alone.

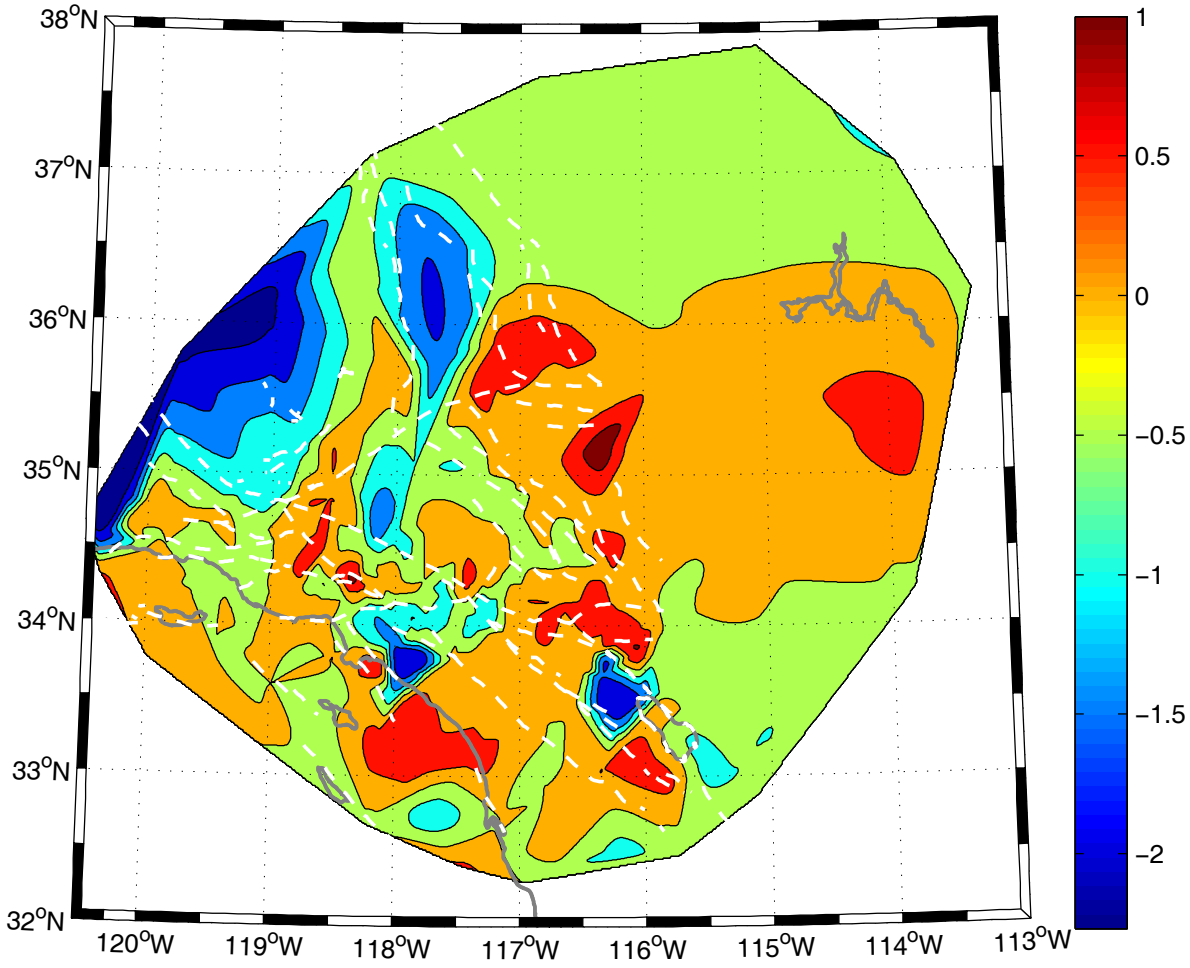


Fig.5-15: Pattern of *vertical* components of the displacement in the Southern *California* in units of mm/yr. Faults are represented by white dashed lines and coastlines are represented by bold solid lines. Figure is illustrated in *Albers Conic Equal-Area Projection* with center of projection at $116.75^0 W / 35^0 N$ with standard parallels $33^0 N$ and $37^0 N$ on reference ellipsoid *GRS*80.

# Chapter 6

## Summary and Conclusions

This chapter summarized the main contributions and results of this research. The advantage and the characteristics of the proposed method of deformation analysis of the Earth surface are critically reviewed. This study has presented the development and implementation of the intrinsic deformation analysis together with eigenspace components of symmetric random deformation tensors (of first and second type) on the *Riemann* manifold $\mathbb{M}^2$. The developed models of the analysis were established upon the observed displacement vectors on the Earth's surface without referring or projecting the vectors on any reference surfaces. The elements of differential geometry of the surfaces are developed in chapter 2.*Lagrangian* and *Eulerian* description of various deformation tensors were introduced in chapter 3 .The description of the tensors obtained as a functions of surface curvilinear components of the displacement vector $\mathbf{u}$ and difference vector of unit normal vectors $\mathbf{w}$ is obtained.. *Gaussian* representation of the Earth surface in terms of the geodetic coordinates with respect to the reference ellipsoid is assumed and invariants of *changing of metric tensor and changing of curvature tensor* and their specific physical meaning are expressed and extracted in chapter 4.The considerable role of these invariants was obvious in chapter 5 through the graphical representations of spatial variations of the deformation tensors field. Moreover the results of intrinsic deformation analysis approach on surface deformation across the Southern *California* based on *Scripps Orbit and Permanent Array Center (SOPAC)* solutions were graphically represented as various spatial patterns. Comparison of the patterns with seismic map of the area suggested how well patterns were able to uncover geodynamical features across this region. The pattern of the *surface maximum shear strain* rate indicated that it is a powerful tool to reveal the high seismicity across the regions surrounding previous earthquakes. The pattern of *rotation around the normal* disclosed that the *rotation tensor* includes desirable information. Comparison of this pattern with the *surface maximum shear strain rate* shows the ability of the *rotation tensor to uncover geodynamic features*. The ability of eigenvalues of *Lagrange deformation tensor of second kind* in representing the high seismicity area was another most important part of this study. The comparison of the patterns between difference of eigenvalues and the patterns with the *surface maximum shear strain rate* indicated that using tensor of second kind is a powerful tool in

earthquake investigations. One of the most interesting results of this study is the spatial pattern of *Gaussian curvature differences* and *mean curvature differences* as invariants *of Lagrange deformation tensor of second kind*. The ability of the patterns to uncover the upward and downward motions of the Earth's surface represented by the curvature tensor is able to provide significant information about the *vertical motions*.

Further studies could be carried out to improve the treat of intrinsic analysis from the viewpoint of statistics. Considering the *random* behaviour of observations of deformation tensor, dealing about the eigenspace components of both surface tensors, first and second kind, will be valuable. Therefore this research can be concern about the *statistical behaviour of invariants*, namely *eigenspace components* of *changing of metric tensor (surface strain tensor)* and *changing of curvature tensor*.

## References

Ahjos T, Uski M (1992) Earthquakes in Northern Europe in 1375–1989. Tectonophysics 207:1–23.

Angelier J (1982) Tectonic analysis of fault slip data sets. J Geophys Res 89: 5835-5848.

Aoki Y, Scholz C (2003) Vertical deformation of the Japanese islands, 1996–1999. J Geophys Res 108, 2257 NO. B5, 2257, doi:10.1029/2002JB002129, 2003

Argus DF, Gordon RG, DeMets CD, Stein S (1989) Closure of the Africa–Eurasia–North America plate motions circuit and the tectonic of the Gloria fault. J Geophys Res 94:5585–5602

Assumpcao M (1992) The regional intraplate stress field in South America. J Geophys Res 97: 11889-11903.

Bada G, Horvath F,Gerner P, Fejes I (1999) Review of the present-day geodynamics of the Pannonian basin, progress and problems. J Geodynam 27:501–527

Bai WM, Vigny C, Ricard Y, Froidevaux C (1992) On the origin of deviatoric stresses in the lithosphere. J Geophys Res 97: 11728-11737

Beavan J, Matheson D,Denys P, Denham M, Herring T, Hager B, Molnar P (2004) A Vertical Deformation Profile across the Southern Alps, New Zealand, from 3.5 Years of Continuous GPS Data, : Proceedings of Workshop, The State of GPS Vertical Positioning Precision: Separation of Earth Processes by Space Geodesy, Cahiers du Centre Européen de Géodynamique et de Séismologie, Vol. 23, eds. T. van Dam and O. Francis, pp. 111-123, Luxembourg, 2004.

Beda G, Kozak I, Verhas J (1995) Continuum mechanics, Academia Kiado, Budapest.

Bennett R A, Rodi W, Reilinger RE (1996) Global Positioning System constraints on fault slip rates in Southern California and northern Baja, Mexico. J Geophys Res 101: 21943-21960.

Bianco G, Devoti R, Fermi M, Luceri V, Rutigliano P, Sciarretta C (1998) A contribution in the estimation of tectonic motion in crucial areas: the CGS96 SLR solution. Tectonophysics 294:225–236

Bock Y, Shimada S (1989) Continuously monitoring GPS networks for deformation measurements, Global and regional geodynamics, International association of geodesy symposium No. 102, Edinburgh (Scotland) pp. 40-56

Boucher C, Altamimi Z, Sillard P (1999) The 1997 International Terrestrial Reference Frame (ITRF97). Tech note 27, IERS, Observatoire de Paris, Paris

Caporali A, Martin S (2000) First results from GPS measurements on present day Alpine kinematics. J Geodynam 30:275–283

Castellarin A, Cantelli L, Fesce AM, Mercier JL , Picotti V, Pinni GA, Prosser G, Selli L (1992) Alpine compressional tectonics in the Southern Alps: relationships with the Apennines. Ann Tecton 6:62–94

Chan WS , Xu YL, Ding XL , Dai WJ (2006) An integrated GPS–accelerometer data processing technique for structural deformation monitoring. J Geod 80:705-719

Chen R (1991) On the horizontal crustal deformation in Finland. Rep Finnish Geod Inst 91:1, Masala

Clarke PJ, Davies RR, England PC, Parsons B, Billiris H, Paradissis D, Veis G,Cross PA., Denys PH, Ashkenazi V, Bingley R, Khale HG, Muller MV , Briole P (1998) Crustal strain in central Greece from repeated GPS measurements in the interval 1989-1997. Geophys J Int 135: 195-214

Cross PA, Hannah J, Hradilek L, Kelm R, Mäkinen J, Merry CL, Sjoeberg LE, Steeves RR, Vanıcek P, Zilkoski DB (1987) Fourdimensional geodetic positioning. Manuscr Geod 12:147–222

DeMets C, Gordon RC, Stein S, Argus DF (1987) A revised estimate of Pacific-North America motion and implications for western North America plate boundary zone tectonics. Geophys Res Lett 14: 911-914.

DeMets C, Dixon T (1999) New kinematic models for Pacific-North America motion from 3 Ma to present, 1: Evidence for steady motion and biases in the NUVEL-1A model. Geophys Res Lett 26: 1921-1924.

Dermanis A, Grafarend EW (1993) The finite element approach to the geodetic computation of two- and three-dimensional deformation parameters: A study of frame invariance and parameter estimability. Proceedings of the international conference on cartography - Geodesy, Maracaibo (Venezuela)

Dewey JF (1988) Extensional collapse of orogens. Tectonics 7:1123–1139.

Donnellan AB, Hager King RW, Herring T (1993)Geodetic measurement of deformation in the Ventura Basin region, Southern California, J Geophys Res 98: 21727-21739.

Eringen AC (1962) Non-linear theory of continuous media. McGraw-Hill, New York.

Ernst LJ (1981) A geometrically nonlinear finite element shell theory. Department of mechanical engineering, Delft University of technology, WTHD 132.

Gasparini C, Iannaccone G, Scarpa R (1985) Fault-plane solutions and seismicity of the Italian Peninsula. Tectonophysics 117:59–78

Goelke M, Cloetingh S, Coblentz D (1996) Finite-element modelling of stress patterns along the Mid-Norwegian continental margin, 62_ to 68_N. Tectonophysics 266:33–53

Grafarend EW, Kleusberg A.,Schaffrin B (1980) An introduction to the variance-covariance-component estimation of Helmert type, ZVF, 161–180

Grafarend EW (1986) Three-dimensional deformation analysis: Global vector spherical harmonics and local finite element representation, Tectonophysics 130:337-359

Grafarend EW, Engels J (1992) A global representation of ellipsoidal heights - geoidal undulations or topographic heights - in terms of orthonormal functions, Part 1: ”amplitude-modified” spherical harmonic functions, manuscript a geodaetica 17 pp. 52-58; Part 2: ”phase-modified” spherical harmonic functions, manuscript a geodaetica 17 pp. 59-64.

Grafarend EW (1995) The optimal universal transverse Mercator projection. Manus Geod 20 :421-468.

Grafarend EW, Voosoghi B (2003) Intrinsic deformation analysis of the Earth's surface based on displacement fields derived from space geodetic measurements. Case studies: present-day deformation patterns of Europe and of the Mediterranean area (ITRF Data Sets). J Geod 77: 303-326

Grafarend EW (2004) Tensor Algebra, Linear Algebra, Multilinear Algebra.Department of Geodesy and Geoinformatics, Univ. of Stuttgart, Technical Report, Nr.2004.1.

Grafarend EW, Krumm FW (2006) Map Projections, Cartographic Information Systems. Springer, Berlin.

James TS, Lambert A (1993) A comparison of VLBI data with ICE-3G glacial rebound model. Geophys Res Lett 20:871–874

Johnson HO, DC Agnew, Wyatt FK (1994) Present-day crustal deformation in Southern California. J Geophys Res 99:23951-23974.

Johansson JM, Davis JL, Scherneck HG, Milne GA, Vermeer M, Mitrovica JX, Bennett RA, Ekman M, Elgered G, Elosegui P, Koivula H, Poutanen M, Rönnäng BO, Shapiro II (2002) Continuous GPS measurements of postglacial adjustment in Fennoscandia, 1, Geodetic results, J Geophys Res 107(B8), 2157, doi:10.1029/2001JB000400

Gowd TN, Rao SVS, Gaur VR (1992) Tectonic stress field in the Indian subcontinent, J Geophys Res 97:11879-11888.

Harada T, Shimura M (1978) Horizontal deformation of the crust in Western Japan revealed from first order triangulation carried out three times. Tectonophysics 52:469–478

Horner F, Freeman R (1983) Paleomagnetic evidence from pelagic limestones for clockwise rotation of the Ionian zone. Western Greece. Tectonophysics 98:11–27

Kahle HG , Straub C, Reilinger R, McClusky S, King R, Hurst K, Veis G, Kasten K, Cross P, 1998. The strain field in the eastern Mediterranean region, estimated by repeated GPS measurements.Tectonophysics 294:237-252.

Kakkuri J (1997) Postglacial deformation of the Fennoscandian crust. Geophysica 31:99–109

Kakkuri J Chen R (1992) On horizontal crustal strain in Finland. Bull Geod66:12–20

Kakkuri J, Wang ZT (1998) Structural effects of the crust on the geoid modeled by using deep seismic sounding interpretations. Geophys J Int 135:495–504

Kostrov BV, Das S (1988) Principles of earthquake source mechanics. Cambridge.

Lesne O, Calais E, Deverchere J (1998) Finite element modelling of crustal deformation in the Baikal rift zone: new insights into the active–passive rifting debate. Tectonophysics 289(4):327–340

Libai A, Simmonds JG (1998) The Nonlinear Theory of Elastic Shells. Cambridge University Press.

Livieratos E (1978) Techniques and problems in geodetic monitoring of crustal movements at tectonically unstable regions. In: Vogel A (ed) Terrestrial and space techniques in earthquake prediction research, Friedr. Vieweg & Sohn, Wiesbaden pp 515–531

Lundgren P, Saucier F, Palmer R, Langon M (1995) Alaska crustal deformation: finite element modeling constrained by geologic and very long baseline interferometry data. J Geophys Res Solid Earth 100:22033–22047

Martin D (1991) Manifold Theory: An introduction for mathematical physicists. Ellis Horwood Limited, Great Britain.

MacMillan DS, Ma C (1999) VLBI measurements of Caribbean and South American motion .Geophys Res Lett 26:919–922

Macvean DB (1968) Die Elementararbeit in einem Kontinuum und die Zuordnung von Spannungs- und Verzerrungstensoren, Zeitschrift für angewandte Mathematic und Physik 19:157-185.

Mazzotti S, Dragert H, Henton J, Schmidt M, Hyndman R , James T , Lu Y, Craymer M (2003) Current tectonics of northern Cascadia from a decade of GPS measurements. J Geophys Res 108,B12 , 2554, doi:10.1029/2003JB002653.

McCarthy DD (1996) IERS Conventions 1996. IERS tech note 21, Observatoire de Paris, Paris

McKenzie DP (1970) Plate tectonics of the Mediterranean region. Nature 226:239–243

Massonnet D, Holzer T, Vadon H (1997) Land subsidence caused by the East Mesa geothermal field, California, observed using SAR interferometry. Geophys Res Lett 24: 901-904.

Miyazaki S, Saito T, Sasaki Y, Hatanaka Y, Limura Y (1997) Expansion of GSI's nationwide GPS array. Bull Geog Surv Inst 43:23–34

Milne GA, Davis JL , Mitrovica JX, Scherneck HG , Johansson JM, Vermeer M,Koivula H (2001) Space-Geodetic Constraints on Glacial Isostatic Adjustment in Fennoscandia, Science, Vol. 291, 23 March 2001, pp. 2381-2385.

Mueller B, Zoback ML, Fuchs K, Mastin L, Gregersen S, Pavoni N, Stephansson O, Ljunggren C( 1992) Regional patterns of tectonic stress in Europe. J Geophys Res 97:11783–11803

Mushtari KhM, Galimov K (1961) The non-linear theory of elastic shells, Israel Program Sci Transl (Translated from Russian)

Naghdi PM (1972) The theory of shells and plates, Handbuch der Physik VI, A2, Springer, Berlin Heidelberg New York

Namson J, Davis T (1998) Structural transect of the Western Transverse Range, California: Implications for lithospheric kinematics and seismic risk evaluation, Geology16:675-679

Nikolaidis R (2002) Observation of Geodetic and Seismic Deformation with the Global Positioning System.Ph.D. Thesis, University of California, San Diego.

Olszak W (1980) The shell theory: new trends and applications.International Center for Mechanical Sciences.Courses and lectures no. 240. Springer, Berlin Heidelberg New York

Pagarete J, Teixeira PJ, Mendes VB, Antunes C, Ribeiro H (1998) The importance of classical geodetic observations for analyzing the geodynamic behaviour of the Acores archipelago.Tectonophysics 294:281–290

Prakash N (1981) Differential geometry. Tata McGraw-Hill publishing Co. Ltd., New Delhi

Pietraszkiewicz W (1977) Introduction to the non-linear theory of shells, Mitteilungen aus dem institut fuer Mechanik Nr 10, Ruhr-Universität Bochum, Germany

Plag HP, Engen B, Clark TA, Degnan JJ, Richter B (1998) Postglacial rebound and present-day three-dimensional deformations, J Geodynam 25:213–240

Pollitz FF, Peltzer G, Burgmann R, Mobility of continental mantle (2000) Evidence from postseismic geodetic observations following the 1992 Landers earthquake, J Geophys Res **105**, 8035-8054

Pollitz FF, Wicks C, Thatcher W (2001) Mantle flow beneath a continental strike-slip fault; postseismic deformation after the 1999 Hector Mine earthquake, Science 293, 1814-1818.

Reilinger RE, McClusky SC, Oral MB, King RW, Toksoz MN (1997a) Global positioning system measurements of present-day crustal movements in the Arabia-Africa-Eurasia plate collision zone. J Geophys Res, 102 No.B5 pp. 9983-9999

Reilinger RE, McClusky SC, Souter BJ (1997b) Preliminary estimates of plate convergence in the Caucasus collision zone from global positioning system measurements. Geophys Res Lett 24:1815-1818

Reissner E (1974) Linear and Nonlinear Theory of Shells. Thin Shell Structures, Y. C. Fung and E. E. Sechler, eds., Prentice-Hall, Englewood Cliffs.

Renner G, Slejko D (1994) Some comments on the seismicity of the Adriatic region. Boll Geofis Teor Appl 36:141–144

Sagiya T, Thatcher W (1999) Coseismic slip resolution along a plate boundary megathrust: the Nankai trough, southwest Japan. J Geophys Res 104:1111–1129

Savage JC, Lisowski M, Prescott WH (1990) An apparent shear zone trending north-northwest across the Mojave Desert into Owens Valley, eastern California. Geophys Res Lett 17 (12):2113-2116

Savage JC, Svarc JL, Prescott WH (2003) Near-field postseismic deformation associated with the 1992 Landers and 1999 Hector Mine, California, earthquakes, J Geophys Res 108 (B9), doi: 10.1029/2002JB002330

Scherneck HG, Johansson JM, Mitrovica JX, Davis JL (1998) GPS determined 3-D displacement rates in Fennoscandia from 800 days of continuous observations in the SWEPOS network. Tectonophysics 294:305–321

Shen-Tu BM, Holt WE, Haines AJ (1999) Deformation kinematics in the western United States determined from Quaternary fault slip rates and recent geodetic data, J Geophys Res, 104, 28927-28955

Shen ZK, Jackson DD, Ge BX (1996) Crustal deformation across and beyond the Los Angeles basin from geodetic measurements, J Geophys Res101: 27957-27 980

Smith DE, Kolenkiewicz R, Dunn PJ, Torrance MH , Klosko SM, Robbins, JW, Williamson RG, Pavlis EC, Douglas NB, Fricke SK (1990) The determination of present-day tectonic motions from laser ranging to LAGEOS, In: Brunner FK, Rizos, C., Developments in Four-Dimensional Geodesy. Ron S, Mather Symposium on Four-Dimensional Geodesy, Sydney, Australia, March 28–31, 1989. Lecture notes in Earth sciences 29, Springer-Verlag, New York pp 221–240

Snay RA, Cline W, Philipp CR. , Jackson DD , Feng Y, Shen ZK (1996) Crustal velocity field near the big bend of California's San Andreas fault, J Geophys Res 101:3173-3185

Soudarin L, Crétaux J (2006) A model of present-day tectonic plate motions from 12 years of DORIS measurements, J Geod 80: 609-624 .

Stein E (1980) Variational functionals in the geometrical nonlinear theory of thin shells and finite element discrimination with applications to stability problems. In: Koiter WT, Mikhailov GK (eds) Theory of shells, North Holland, Amsterdam, pp 241–262.

Stein RS, King GCP , Lin J (1994) Stress triggering of the 1994 *M*=6.7 Northridge, California, earthquake by its predecessors, Science, 265, 1432-1435.

Thomas AP, Rockwell TK (1996) A 300- to 500-year history of slip on the Imperial Fault near the U.S. –Mexico border: Missing slip at the Imperial fault bottleneck, J Geophys Res, 101, 5987– 5997

Terada T, Miyabe N (1929) Deformation of earth crust in Kiranasai District and its relation to the orographic feature, Bull Earth Res Inst 7:223–241

Tregoning P, Lambeck K, Stolz A, Morgan P, McClusky S, Beek P, McQueen H, Jackson RJ, Little RP, Laing A , Muphy B (1998) Estimation of current plate motions in Papua New Guinea from Global Positioning System observations, J. Geophys. Res., Vol.103, B6 pp.12181-12203

Tsuboi C (1930) A note on the analytical treatments of the horizontal deformation of the earth crust. Bull Earth Res Inst 8:384–392

Vanbrabant Y, Jogmans D, Hassani R, David B (1999) An application of two-dimensional finite element modelling for studying the deformation of the variscan fold-and-thrust belt (Belgium), Tectonophysics 309(1–4):141–159

Vanicek P, Thapa K, Schneider D (1981) The use of strain to identify incompatible observations and constraints in horizontal geodetic networks, Manuscr Geod 6:257–281

Visconti A (1992) Introductory differential geometry for physicists, World Scientific Publishing Co. Pte.Ltd., Singapore

Wald D, Heaton T, Hudnut K (1996) The slip history of the 1994 Northridge, California, earthquakes determined from strong ground motion, teleseimic, GPS, and leveling data, Bull. Seismo. Soc. Am., 86, S49-S70

Ward ST (1998a) On the consistency of earthquake moment rates, geological fault data, and space geodetic strain: the United States. Geophys J Int, 134 No.1 pp. 172-186

Ward ST (1998b) On the consistency of earthquake moment release and space geodetic strain rates: Europe. Geophys J Int, 135 No.3 pp. 1011-1018.

Wdowinski S, Sudman Y, Bock Y (2001)Distribution of interseismic deformation along the San Andreas fault system, Southern California, Geophys Res Lett , 28, 2321–2324

Wessel P, Smith WHF (1998) New, improved version of Generic Mapping Tools released. EOS Trans Am Geophys Un 79:579

Wu P (1998) Intraplate earthquakes and postglacial rebound in eastern Canada and Northern Europe, Geores Forum 3–4:603– 628

Zaiser J (1984) Ein dreidimensionales geometrisch-physikalisches Modell f¨ur konventionelle Beobachtungen- Beobachtungsfunktionale, Parametersch¨atzung und Deformationsanalyse, Deutsche Geod¨atische Kommission, Bayerischen Akademie Wissenschaften, Reihe C, Heft Nr. 298